ABSTRACT

MULTIFRACTAL ANALYSIS OF HEART RATE VARIABILITY USING WAVELET-TRANSFORM MODULUS-MAXIMA METHOD

by
Chirag N. Jani

Physiological signals are complex and carry information of human health. Recent studies reveal that under normal conditions, the heart rate time series shows multifractal behavior. In contrast, HRV in the pathological state such as congestive heart failure exhibits more monofractal-like structure. Recent advances in the assessment of heart rate variability (HRV) uses a nonlinear dynamics approach. In this study, the main objective is to use the wavelet-transform modulus-maxima method for the multifractal analysis of the heart rate time series.

The degree of the multifractality is defined by the singularities (a point in time series where a mathematical function is not differentiable). For monofractal signals, the output of a system contains the same type of singularities regardless of the initial condition, while multifractal signals generate outputs with different fractal properties that depend on the input conditions. That is, the output of the system over extended periods of time will display different types of singularities [7]. Multifractality in the heart rate signal is evaluated by the singularity spectrum, which can be found by the local maxima in WTMM method (a method of multifractal analysis that calculates the singularity spectrum to differentiate between normal subjects and congestive heart failure subjects). The multifractal analysis by the WTMM method calculates the spectrum of singularities. For healthy subjects, the singularity spectrum is wide with non-zero singularities. On the other hand, for congestive heart failure subjects the singularity spectrum is a very narrow

range. Moreover, multifractal analysis method provides the calculation of the scaling exponent ($\tau(q)$). For healthy subjects, the $\tau(q)$ spectrum displays nonlinear behavior, while the $\tau(q)$ spectrum is linear for congestive heart failure subjects.

To validate the theory, analysis was performed on 50 subjects and we are clearly able to identify normal and congestive heart failure subjects using the WTMM method of multifractal analysis.

MULTIFRACTAL ANALYSIS OF HEART RATE VARIABILITY USING WAVELET-TRANSFORM MODULUS-MAXIMA METHOD

By
Chirag Jani

A Thesis
Submitted to the Faculty of
New Jersey Institute of Technology
in Partial Fulfillment of the Requirements for the Degree of
Master of Science in Biomedical Engineering

Department of Biomedical Engineering

August 2005

APPROVAL PAGE

MULTIFRACTAL ANALYSIS OF HEART RATE VARIABILITY USING WAVELET-TRANSFORM MODULUS-MAXIMA METHOD

Chirag Jani

Dr. Stanley Reisman, Thesis Advisor — Date
Professor of Biomedical Engineering, NJIT

Dr. Ronald Rockland, Committee Member — Date
Associate Professor of Engineering Technology, NJIT

Dr. Tara Alvarez, Committee Member — Date
Assistant Professor of Biomedical Engineering, NJIT

BIOGRAPHICAL SKETCH

Author: Chirag N. Jani

Degree: Master of Science

Date: August 2005

Graduate and Undergraduate Education:

- Master of Science in Biomedical Engineering
  New Jersey Institute of Technology, Newark, New Jersey, 2005

- Bachelor of Science in Computer Science
  University of Houston-Clear Lake, Houston, Texas, 2003

Major: Biomedical Engineering

To my beloved family
Your faith is my encouragement.
Your support is my strength.
Your love is my inspiration.
Your motivation is my success.

Thank You…

ACKNOWLEDGEMENT

I would like to express my deepest appreciation to Dr. Stanley Reisman for his motivation, invaluable guidance and personal attention. I would like to appreciate him for providing precious resources and inspiration.

I thank Dr. Tara Alvarez and Dr. Ronald Rockland for being my thesis committee members. I thank all my colleagues working in the lab for the exchange of knowledge specially Nirvish Shah, Hardik Raval and Diane Donnelly. I would really like to thank Kapil Anand for providing me his computer and heart rate data. Also, I thank my parents for providing me financial and moral support. I thank God for keeping my existence on the earth.

TABLE OF CONTENTS

TABLE OF CONTENTS
(Continued)

Chapter **Page**

LIST OF TABLES

LIST OF FIGURES

LIST OF FIGURES
(Continued)

CHAPTER 1

INTRODUCTION

This chapter provides an overview of the study, and locates it within the different methods of nonlinear dynamics particularly multifractal analysis. In addition, it describes the specific aims of the study and the structure of this thesis.

1.1 Objective

During the last two decades, a great deal of work has been devoted in understanding the physiological information behind the variability of the cardiac cycle. Even though well established analysis tools from linear system theory can provide valuable information for physiological and clinical interpretation of the HRV, it has been speculated that methods from nonlinear dynamics may provide a powerful tool to deduce more information for better understanding the mechanisms of cardiovascular control [7].

The primary goal of this study is to extend the knowledge of research from the linear to the nonlinear methods and examine nonlinear techniques that extract more knowledge and features out of them. New emerged techniques of nonlinear dynamics have brought new approach to the analysis of heart rate variability (HRV) that might help to uncover human health. The method that has been studied in this thesis is multifractal analysis.

This study was conducted with a goal to investigate the efficacy of the WTMM method (a method of multifractal analysis that calculates the singularity spectrum to

differentiate between normal subjects and congestive heart failure subjects) and test the significance of the obtained results and derived graphs.

1.2 Structure of Thesis

The structure of the thesis explains the step-by-step approach towards the objective.

Chapter 1 summarizes the objective of the thesis involving the contribution of nonlinear dynamics and nonlinear methods on heart rate variability.

Chapter 2 summarizes the physiological and engineering background of the cardiovascular system. The anatomy of the heart, the electrocardiogram (ECG), RR-interval, heart rate variability, effect of the nervous system on the heart rate variability, chaos theory and characteristics of fractals are presented.

Chapter 3 provides detailed explanation on the multifractal analysis. Available tools and methods used to describe multifractal analysis of the RR time series are mentioned in this chapter and have been used as a basis of our analysis.

Chapter 4 provides data acquisition, analysis and discussion of the obtained results. Different tests have been performed to differentiate two groups- NSR group (normal subjects) and CHF group (congestive heart failure group).

Chapter 5 ends the thesis with conclusions as well as suggestion of topics for future study.

CHAPTER 2

PHYSIOLOGICAL AND ENGINEERING BACKGROUND

Heart rate variability provides vital basis to comprehend the human health. To grasp the understanding of HRV, knowledge of cardiovascular system and autonomic nervous system is essential.

2.1 Physiology of the Heart

The heart is a part of the circulatory system and composed of cardiac muscle tissue, which constantly pumps blood throughout the body. Cardiac muscle tissue is very strong and able to contract and relax rhythmically throughout a person's lifetime.

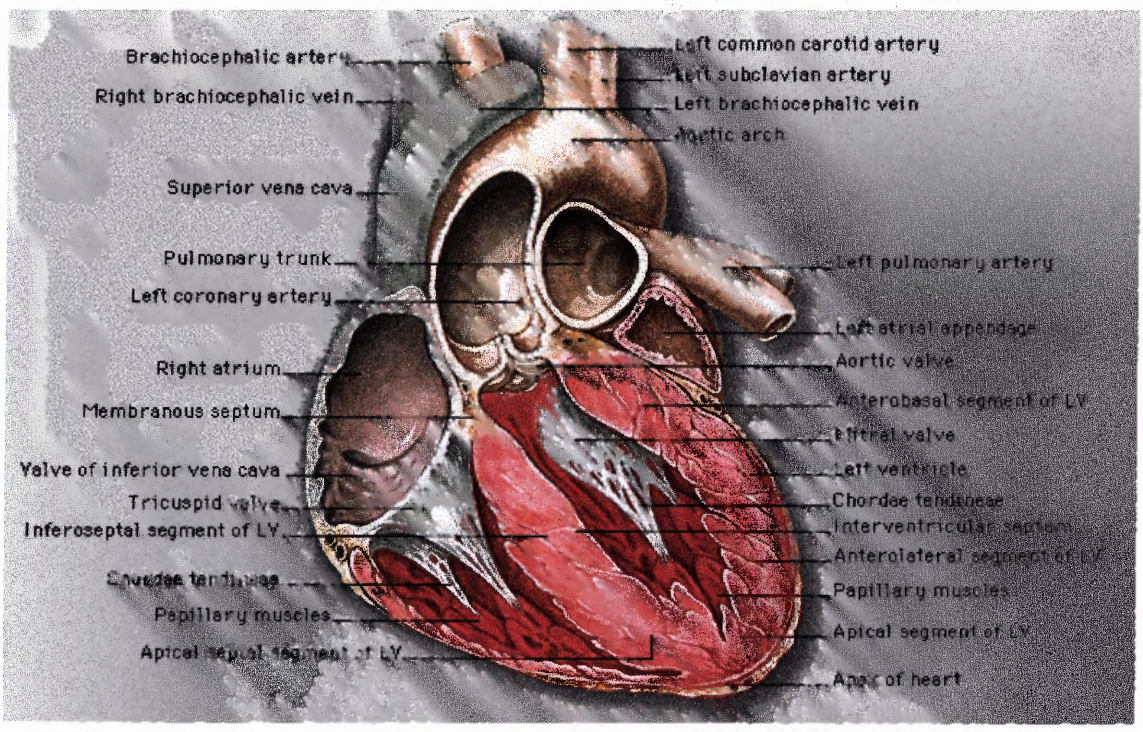

Figure 2.1 The heart [1].

The human heart is considered as two pumps in one. The right side receives oxygen-poor blood from the various regions of the body and delivers it to the lungs. In the lungs, oxygen is absorbed in the blood. The left side of the heart receives the oxygen-rich blood from the lungs and delivers it to the rest of the body.

As one can see in Figure 2.1, the heart has four chambers. The upper chamber on each side of the heart is called the atrium, which receives and collects the blood coming to the heart. The atrium then delivers blood to the lower chamber, called a ventricle, which pumps blood away from the heart through rhythmic contractions. A network of nerve fibers coordinates the contraction and relaxation of the cardiac muscle tissue to obtain an efficient, wave-like pumping action of the heart [2].

The Sinoatrial Node, SA-node, located at the junction of the right atrium and the superior vena cava serves as the natural pacemaker for the heart. Nestled in the upper area of the right atrium, it sends the electrical impulse that triggers each heartbeat. The impulse spreads through the atria, prompting the cardiac muscle tissue to contract in a coordinated wave-like manner.

The impulse that originates from the SA-node strikes the Atrioventricular Node (AV node) that is situated in the lower portion of the right atrium. The AV node sends an electrical impulse to the bottom of the ventricle via the bundle of His and then signal is transmitted all over the ventricle by the Purkinje fibers that cause the cardiac muscle tissue to contract [3].

2.2 Electrocardiography and ECG Signal

Since body fluids are good conductors, generated electrical current by the conduction activity of the heart spread throughout the body and can be picked up on the body surface, amplified, and recorded with an instrument called an electrocardiograph. The graphic recording of electrical changes during this heart's electrical activity is called an electrocardiogram (ECG) [4].

The electrical activity of the heart is a sequence of depolarization and repolarization. Depolarization occurs when the cardiac cells, which are electrically polarized, lose their internal negativity by the efflux of Ca^{+2}. The spread of depolarization travels from cell to cell, producing a wave of depolarization across the entire heart. This wave represents a flow of electricity that can be detected by electrodes placed on the surface of the body. Once depolarization is complete, the cardiac cells are restored to their resting potential, which is called repolarization. Figure 2.2 shows the electrical waves due to the electrical activity of the heart.

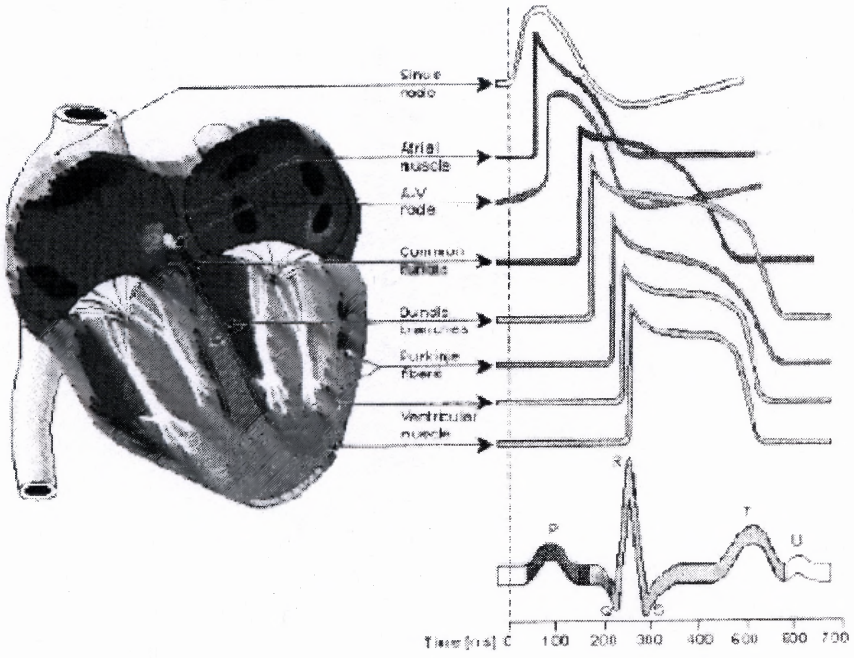

Figure 2.2 Electrical activities from the various region of the heart [37].

Due to the depolarization and repolarization, each heart beat results in three waves or deflections on an ECG. The electrical activation (depolarization) of the upper chambers of the heart (the atria) results in the low amplitude P wave. The subsequent electrical activation (depolarization) of the lower chambers of the heart (the ventricles) results in the high amplitude QRS complex. Repolarization of the atria is a low amplitude signal that occurs during the time of the high amplitude QRS and consequently, is not seen on a standard ECG. Replolarization of the ventricles results in the T wave as shown in Figure 2.2. The flat lines before the P wave, between the P and QRS and after the T wave are said to be at the baseline of that ECG tracing. The line connecting the QRS to the T wave is called the ST segment and is normally quite close to the baseline.

The voltage of the P wave and QRS complex is proportional to the total amount of muscle being depolarized. A higher than normal voltage implies overgrowth of the muscle of that chamber. Since the left ventricle has a lot more muscle than the right ventricle, the QRS complex primarily represents electrical events of the left ventricle [7]. One can calculate the heart rate by dividing 60,000 by the time (in milliseconds) between two consecutive R waves [6].

2.3 RR Interval

Time duration between two consecutive R waves of the ECG is called the RR interval [7].

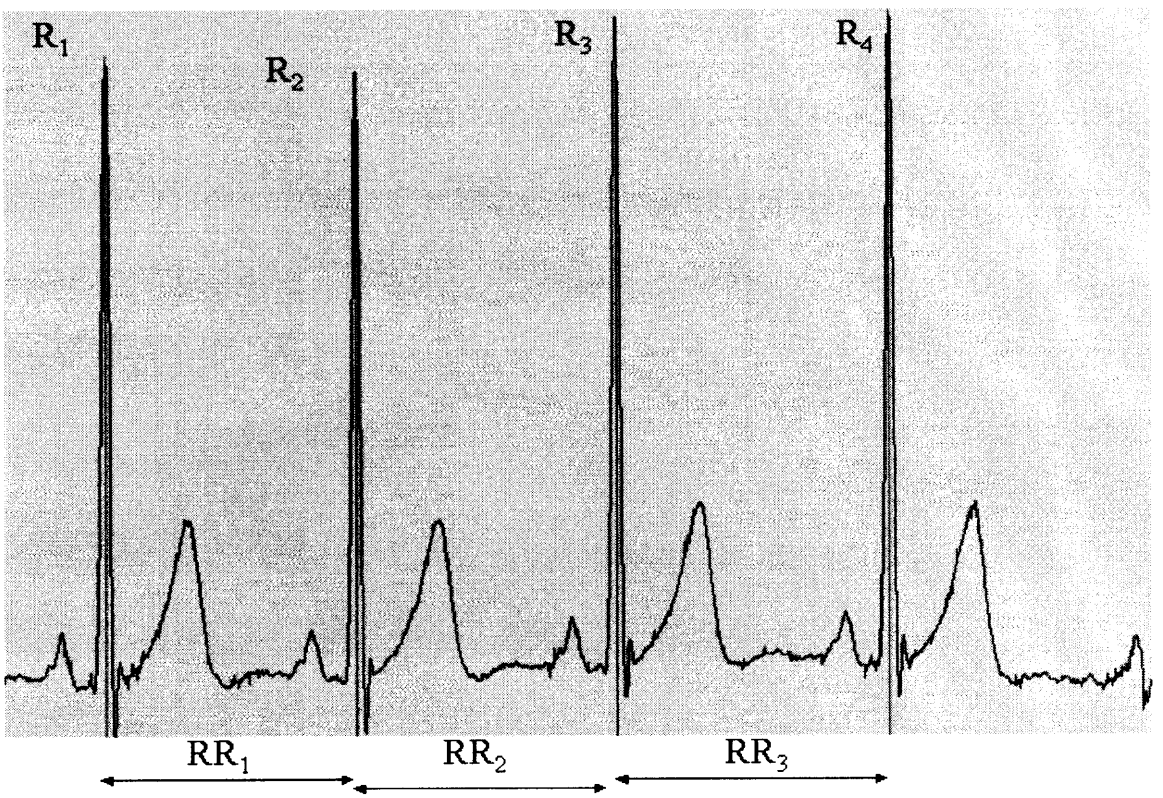

Figure 2.3 ECG signal and RR interval [8].

RR intervals can be derived from an ECG signal very easily. First, the time of occurrence of the R peak is identified for each heart-beat (red lines in Figure 2.3). The difference between the times of occurrence of the $(n+1)^{th}$ beat and the n^{th} beat is then called RR-interval of the n^{th} beat.

2.4 The Cardiovascular Control System

The understanding of the cardiovascular control system is very complex. It requires involvement of several control mechanisms and a variety of receptors. Figure 2.2 provides a functional illustration of the control mechanisms of the cardiovascular control and its constituents.

The Autonomic nervous system has major effect on the heart and heart rate variability. The nervous system is composed of all nerve tissues in the body. The functions of nerve tissue are to receive stimuli, transmit stimuli to nervous centers, and to initiate response. There are two parts of the nervous system: the central nervous system and the peripheral nervous system. The peripheral (sensory) nervous system receives stimuli, the central nervous system interprets them, and then the peripheral (motor) nervous system initiates responses. The somatic nervous system controls functions that are under conscious voluntary control such as skeletal muscles and sensory neurons of the skin. The autonomic nervous system, mostly motor nerves, controls functions of involuntary smooth muscles, cardiac muscles, and glands. The autonomic nervous system provides almost every organ with a double set of nerves –the sympathetic and parasympathetic. These systems generally but not always work in opposition to each

other. Main concern of this study will be limited to the autonomic nervous system and its effect on the heart.

The sympathetic system activates and prepares the body for vigorous muscular activity, stress, and emergencies. The parasympathetic system lowers activity, operates during normal situations, permits digestion, and conservation of energy.

The two systems generally act in opposition to each other. For example, stimulation by the sympathetic system on the heart would increase contractions, while stimulation by the parasympathetic system would decrease heart contractions. Where dual control of an organ exists, both systems operate simultaneously although one may be operating at a higher level of activity than the other.

The following section will explain the effect of the different neurotransmitters and receptors on the heart rate and control loops. Control loop is a term used in the theory of control systems to describe the basic control scheme. This scheme includes a sensor, which detects changes in the parameter under control, and an effector, which alters the parameter in the opposite direction to the change detected by the sensor.

The Autonomic Nervous System (ANS) is an important part of the control loops responsible for the regulation of the heart rate. As was mentioned before, the ANS is divided into two subsystems: the sympathetic and parasympathetic systems. The different functions of the ANS dictate both the anatomical and physiological structure of the sympathetic and parasympathetic systems. Nerve fibers of the sympathetic system leave the central nervous system at ganglia near the spinal cord, while nerve fibers of the Parasympathetic system leaves the central nervous system through cranial nerves (III, VII, IX and X) and through the sacral portion of the spinal cord.

The main neurotransmitter of both systems is acetylcholine, which is also secreted at the endings of parasympathetic nerves. In the sympathetic nervous system, most nerve endings secrete norepinephrine and the receptors, which are sensitive to this neurotransmitter, are called adrenergic receptors. Sympathetic and parasympathetic activation have opposing effects on most organs. In normal conditions, both the sympathetic and the parasympathetic systems maintain a certain level of activity. Therefore, stimulation of one system is equivalent, to some degree, to the stimulation of the other one [9].

In the organs, the receptors to norepinephrine are divided into two subgroups: α and β receptors. The β receptors are further divided into two types: β1 and β2 receptors. The intricate structure of the ANS is well suited for the functions of its two branches. During stress and emergency, organs must respond in various ways, and moreover, the same kind of tissue (such as blood vessels) located in different places must react differently to the same stimulations. The presence of the several types of receptors enables body to recruit for action using activation of the sympathetic system. The sympathetic system can stimulate adrenergic receptors by activation of the adrenal medulla, a gland located on the kidney that secretes both epinephrine and norepinephrine into the circulation. The epinephrine and norepinephrine, which are part of a group of substances called catecholamines, have the same effect as caused by direct neural stimulation, except that their effect lasts 5 to 10 times as long.

The effect of autonomic stimulation on the heart depends on the specifically activated autonomic branch. Activation of the parasympathetic system as well as inhibition of the sympathetic system causes a reduction of heart rate and contractility,

concomitantly with a dilation of the coronary arteries. On the other hand, activation of the sympathetic system or inhibition of the parasympathetic system results in increased heart rate and contractility [9].

The heart is innervated by the parasympathetic system via the Vagus (cranial nerve X), and therefore the adjective vagal is often used, meaning parasympathetic innervations of the heart.

Following explanation will show how control system of the cardiovascular system works. Basically, the cardiovascular control system controls heart rate by maintaining a constant blood pressure in the arterial system. Basically blood flow determines the blood pressure [7]. The flow of the blood is given by Poiselle's law.

$$\text{flow} = \frac{\text{pressure}}{\text{resistance}} \tag{2.1}$$

Regulation in blood flow through alterations in the blood pressure requires complex control mechanisms to maintain adequate blood flow throughout the body.

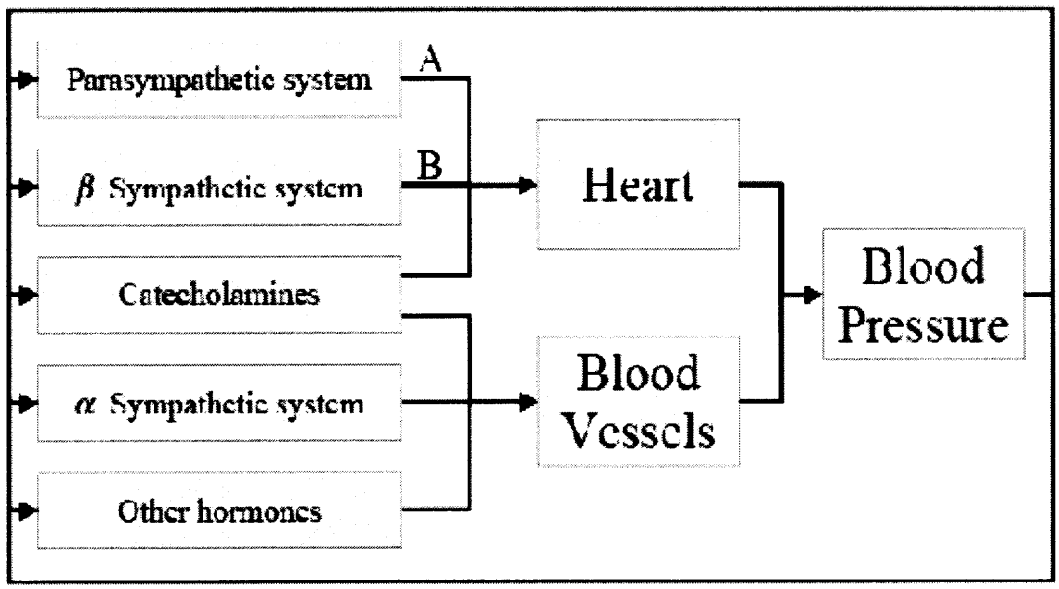

Figure 2.4 A functional block-diagram of cardiovascular control. The main short-term mechanism that regulates the heart rate [9].

This complexity can be removed by the structural advantage of maintaining blood pressure at a constant level and adjusting blood flow by changing resistance. Changes in total resistance must be compensated by opposite changes in cardiac output, in order to keep blood pressure constant. Cardiac output is determined by many factors such as heart rate, stroke volume (the volume of blood ejected by the heart in each beat) and contractility, or the strength of contraction. Heart rate is determined by the cardiac pacemaker-SA node. The SA-node has an intrinsic rate of about 90 BPM and it changes its rate in response to neural stimulation. Stroke volume is determined by the amount of blood entering the left ventricle during diastole. Diastole is the relaxation of the cardiac muscle tissue in the ventricles so that ventricles have more room to accept the blood from the atria. Contractility is determined by the same mechanisms that affect the heart rate. In addition, contractility is also positively dependent on the stroke volume: increased stroke volume results in increased contractility and vice versa. The control loops (this

term is used in the theory of control system to describe the basic control scheme) of the cardiovascular system are classified as either a short term or a long term, according to their behavior in time with respect to stimulation. The control loop includes a sensor, which detects changes in the parameter under control, and an effector, which alters the parameter in the opposite direction to the change detected by the sensor. Short-term control loops respond immediately to changes in blood pressure and their effect lasts for minutes to several hours, while long-term mechanisms respond to changes in blood pressure within hours or days. The various control loops act together to regulate blood pressure.

As the main focus of this study is HRV, concentration is put on the control mechanisms that affect the heart rate. The baroreceptor reflex is the most prominent short-term control mechanism that regulates heart rate through changes of the blood pressure. A baroreflex is a reflex triggered by the stimulation of a baroreceptor (a collection of sensory nerve endings in the wall of the heart auricles, vena cava, aortic arch and carotid sinuses that are specialized to monitor changes in blood pressure). The signals transmitted from the baroreceptors are carried by the cranial nerves to the tractus solitarius in the brain stem. As an example, increase in arterial pressure causes a parallel, although nonlinear, increase in the firing rate of the baroreceptors, and that increase, processed in the brain stem, results in stimulation of the parasympathetic system. As a result, heart rate is reduced.

Several other control mechanisms are Chemoreceptors and humoral control. Chemoreceptors are nerve endings located in the carotid sinus and the aortic arch. Those receptors increase their firing rate in response to either reduction of the oxygen levels in

the blood, or increase of the CO_2 or H^+. These receptors participate not only in the regulation of the oxygen levels and acidity but also in the regulation of the heart rate through the changes of the blood pressure.

Humoral control over blood pressure includes Epinephrine (adrenaline) and norepinephrine (noradrenaline) agents and angiotensin hormone that plays an important role in long-term blood pressure regulation and heart rate. This hormone causes vasoconstriction, thereby increasing blood pressure [9]. As a result heart rate is increased too.

Thus, baroreceptor, chemoreceptor and humoral control influences give origin to heart rate oscillation with a longer period (minutes and hours), which introduces heart rate variability.

2.5 Heart Rate Variability (HRV)

Heart rate variability (HRV) is the fluctuations of the heart rate around its mean value [7]. The spectral structure of the heart rate signal provides essential information regarding the analysis of the HRV. However, it does not supply complete information to observe the effect of the sympathetic nervous system. When one analyzes the power spectrum of the heart rate, it exhibits two main spectral peaks, which are correlated with the ANS activity. Figure 2.5 shows a typical heart rate trace and its corresponding power spectrum.

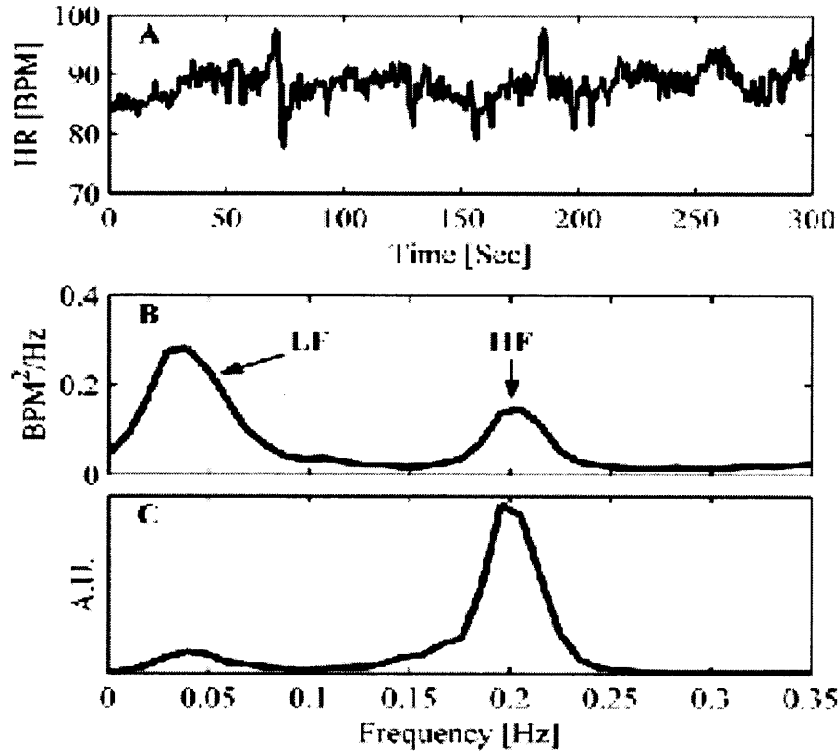

Figure 2.5 An example of the normal heart rate trace (panel-A), and its corresponding power spectrum (panel-B). Panel-C shows the power spectrum of the respiration [9].

As can be seen in the Figure 2.5, the first peak is centered around 0.1 Hz and found in the Low Frequency (LF) band while second peak is centered around the respiratory frequency. Since second peak contains relatively higher frequency than the first peak, it is called HF peak. The relations between autonomic activity and the spectral peaks have been validated in numerous studies, both in humans and in animal models [10]. The understanding of the origin and physiological significance of the two peaks has been mentioned in the literature and concluded that the HF peak has been related to the activity of the parasympathetic system, and the LF peak related to both the sympathetic and parasympathetic systems [10]. Analysis of HRV is a noninvasive tool for assessing cardiac autonomic activity, which is invaluable for the study of human physiology and

pathophysiology.

HRV is not only a measurement of the interaction between sympathetic and parasympathetic activity in autonomic functioning but also provides vital support to investigate the health of a person. There are two main HRV approaches: time domain analysis and frequency domain analysis. These methods are explained in detail in Chapter 3. Since it is very hard to evaluate human health condition by the traditional techniques of the frequency domain and time domain, the nonlinear methods have been introduced in the study of HRV.

2.6 Chaos and HRV

Chaos theory was under development when heart rate variability was being increasingly discussed as a tool for risk stratification after myocardial infraction. The extent to which chaos relates to physiological dynamics is a subject of active investigation and some controversy. At first, it was widely assumed that chaotic fluctuations were produced by pathological systems such as cardiac electrical activity during atrial or ventricular fibrillation [11]. However, this initial presumption has been challenged [12] and the weight of current evidence does not support the view that the irregular ventricular response in atrial fibrillation or that ventricular fibrillation itself represents deterministic cardiac chaos [13]. Further, there is no convincing evidence that other arrhythmias sometimes labeled "chaotic," such as multifocal atrial tachycardia, meet the technical criteria for nonlinear chaos. An alternative hypothesis is subtle but complex heart rate fluctuations observed during normal sinus rhythm in healthy subjects, even at rest, are due in part to deterministic chaos, and that a variety of pathologies, such as congestive

heart failure syndromes, may involve a paradoxical decrease in this type of nonlinear variability.

Chaos is an erratic behavior. However, it is extremely sensitive to initial conditions. Chaos is distinct from periodicity and randomness, but it has characteristics of both. Chaotic behavior looks disorganized, but it is deterministic. Chaos also predicts the long-term system behavior. A chaotic system can actually develop in a way that appears very smooth and ordered [30].

Chaos theory describes complex motion and the dynamics of sensitive systems. Chaotic systems are mathematically deterministic but nearly impossible to predict such as heart rate variability. Chaos is more evident in long-term systems than in short-term systems. Behavior in chaotic systems is aperiodic, meaning that no variable describing the state of the system undergoes a regular repetition of values. Chaos refers to the issue of making accurate long-term predictions of any system if the initial conditions are known to an accurate degree.

Because the mathematical algorithms designed for detecting chaos are not reliably applied to nonstationary (nonstationary- the mean, standard deviation, and higher moments, or the correlation functions are not invariant under time translation), relatively short and often noisy data sets obtained from most clinical and physiological studies, the intriguing question of the role, if any, of chaos in physiology or pathology remains unresolved [5]. In recent years, increasing efforts were made to determine the chaotic nature of cardiac activity by applying analysis methods from nonlinear systems theory. Figure 2.6 shows the heart rate of the normal subject and congestive heart failure subject. As can be seen, both time series have identical means and variances even though they

carry totally different information in the time series. These types of statistical information can lead to the erroneous results. However, methods of nonlinear dynamics provide better way to analyze a signal.

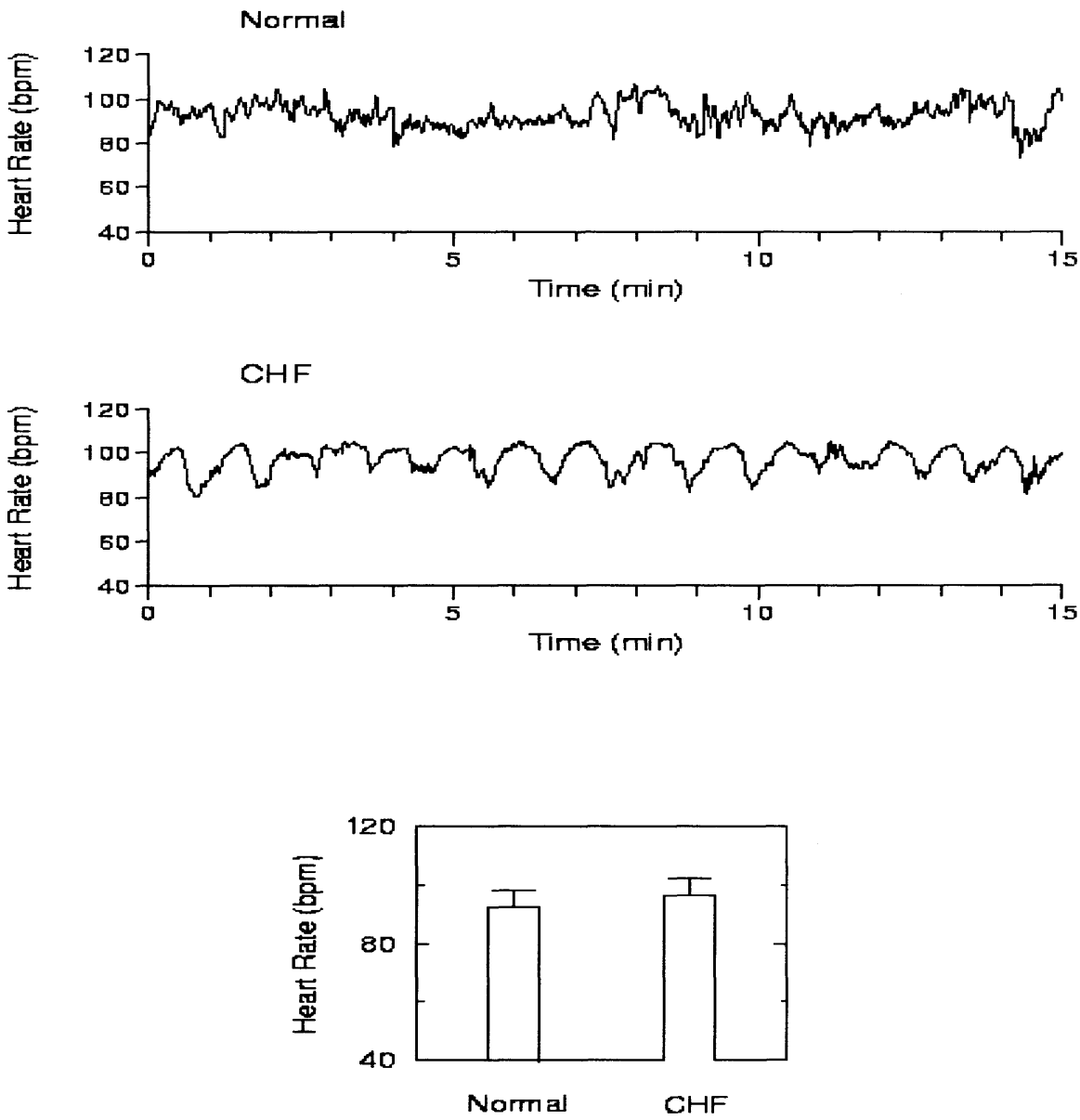

Figure 2.6 (top) The heart rate time series from healthy subject; (middle) the heart rate time series from a patient with severe congestive heart failure; (bottom) identical means and variances of top and middle time series [5].

Chaos theory has some difficulties due to the noisy nature of the biological signals, the restricted length of data and non-stationarity in the signal. These fundamental difficulties have weakened the application of chaos theory in the analysis of HRV. This has led to a shift of the notation from chaos to the development of measures and analysis techniques related to nonlinear dynamics. Examples of such techniques are approximate entropy, renormalized entropy, binary entropies, multifractal analysis and 1/f spectral analysis. There has been an increase in studies demonstrating that nonlinear measures may reveal clinically relevant aspects of heart period or heart rate dynamics, which are not apparent in the analysis of the time and frequency domain.

Since we are going to look into the nonlinear methods of the HRV, it is better to understand the nonlinear system first. The knowledge of nonlinear system is obtained by comparing nonlinear system to the linear systems in this paragraph. A system is linear if its response is directly proportional to excitation, for every part of the system. Two central features of linear systems are proportionality and superposition. Proportionality means that the output shows a straight-line relationship to the input. Superposition refers to the fact that the behavior of linear systems composed of multiple components can be fully understood and predicted by dissecting out these components and figuring out their individual input-output relationships. The overall output will simply be a summation of these constituent parts. In contrast, nonlinear systems violate the principles of proportionality and superposition. Nonlinear system changes the output as a function of sequential time steps and it can be plotted by a feedback procedure. Nonlinear systems or Equations, depending on a value of the single parameter, can generate steady states, regular oscillations, or highly erratic behavior [5]. Thus, for nonlinear systems,

proportionality does not hold and small changes can have dramatic and unanticipated effects. Nonlinear systems that appear to be very different in their specific details may exhibit certain common patterns of response. Sometimes in nonlinear systems, a very small increase or decrease in the value of some parameter controlling the system causes it to change abruptly from one type of behavior to another (bifurcation) and brings the sudden appearance of regular oscillations that alternate between two values. This type of dynamic may cause a variety of alternans patterns in cardiovascular dysfunction. A familiar example is the beat-to-beat alternation in QRS axis and amplitude seen in some cases of cardiac tamponade [13]. Moreover, nonlinear systems composed of multiple subunits cannot be understood by analyzing their constituent components individually. In a nonlinear system, the constituent components interact with each other. Their nonlinear coupling generates behaviors that defy explanation using traditional linear models. As a result, they may exhibit behavior that is characteristic of nonlinear systems, such as self-sustained, periodic waves (e.g., ventricular tachycardia), abrupt changes (e.g., sudden onset of a seizure) and, possibly, chaos.

As was mentioned before, methods of nonlinear dynamics were introduced which uses the concept of fractals. Since chaotic trajectories are fractals, we can relate chaos to the fractals and overcome the mentioned restrictions by a study of fractals in nonlinear methods.

2.7 Fractals

Some physiologic systems show erractic fluctuations resembling those found in dynamical systems driven away from a single equilibrium state. These type of physiologic signals illustrates fractal type behavior. While fractals are irregular, not all irregular structures or erratic time series are fractal. A key feature of the class of fractals seen in biology is a distinctive type of long-range order. This property generates *correlations* that extend over many scales of space or time.

2.7.1 Fractal Objects and Self-similar Processes

Before describing the fractality and multifractality in heart rate variability, we will first understand the meaning of the term fractal. The term fractal is a geometric concept related to, but not synonymous with chaos. The concept of a fractal is most often associated with geometrical objects satisfying two criteria: self-similarity and fractional dimensionality. Self-similarity means that an object is composed of sub-units and sub-sub-units on multiple levels that resemble the structure of the whole object [14]. Mathematically, this property should hold on all scales. However, in the real world, there are necessarily lower and upper bounds over which such self-similar behavior applies. Fractals are irregular structure, but not all irregular structures or erratic time series are fractals. The fractal object has a fractional dimension. This fractal dimension measure distinguishes the fractals from the Euclidean objects. Euclidean objects contain interger dimension whereas the fractals contain noninterger dimension. For example, a solid cube is self-similar since it can be divided into sub-units of 8 smaller solid cubes that resemble the large cube, and so on. However, the cube (despite its self-similarity) is not a fractal

because it has an integer dimension of three (Chapter 3 explains the measurement techniques of the fractal dimensions).

The detection and quantification of the self-similarity in complex time series is a complecated process. Time series are usually plotted on a two-dimensional surface and plotted in a two-dimensional curve. To determine if a two-dimensional curve is self-similar, we can take a subset of the object and rescale it to the same size of the original object, using the same magnification factor for its width and height; and then compare the statistical properties of the rescaled object with the original object.

Mathematically we can say, a time series is self-similar if

$$y(t) \stackrel{d}{\equiv} a^{\alpha} y\left(\frac{t}{a}\right) \tag{2.2}$$

where $\stackrel{d}{\equiv}$ means that the statistical properties of both sides of the equation are identical. In other words, a self-similar process, $y(t)$, with a parameter α has the identical probability distribution as a properly rescaled process, $a^{\alpha}y(t/a)$, i.e., a time series which has been rescaled on the x-axis by a factor t/a and on the y-axis by a factor of $a^{\alpha}y$. The exponent α is called the self-similarity parameter [15].

In the real world, it is impossible to determine whether two processes are statistically identical, because one can not obtain identical mean, variance and other higher moments due to the noise. Therefore, one usually approximates this equality with a weaker criterion by examining only the first moment- means and the second moment - variances of the distribution functions for both sides of Equation 2.2.

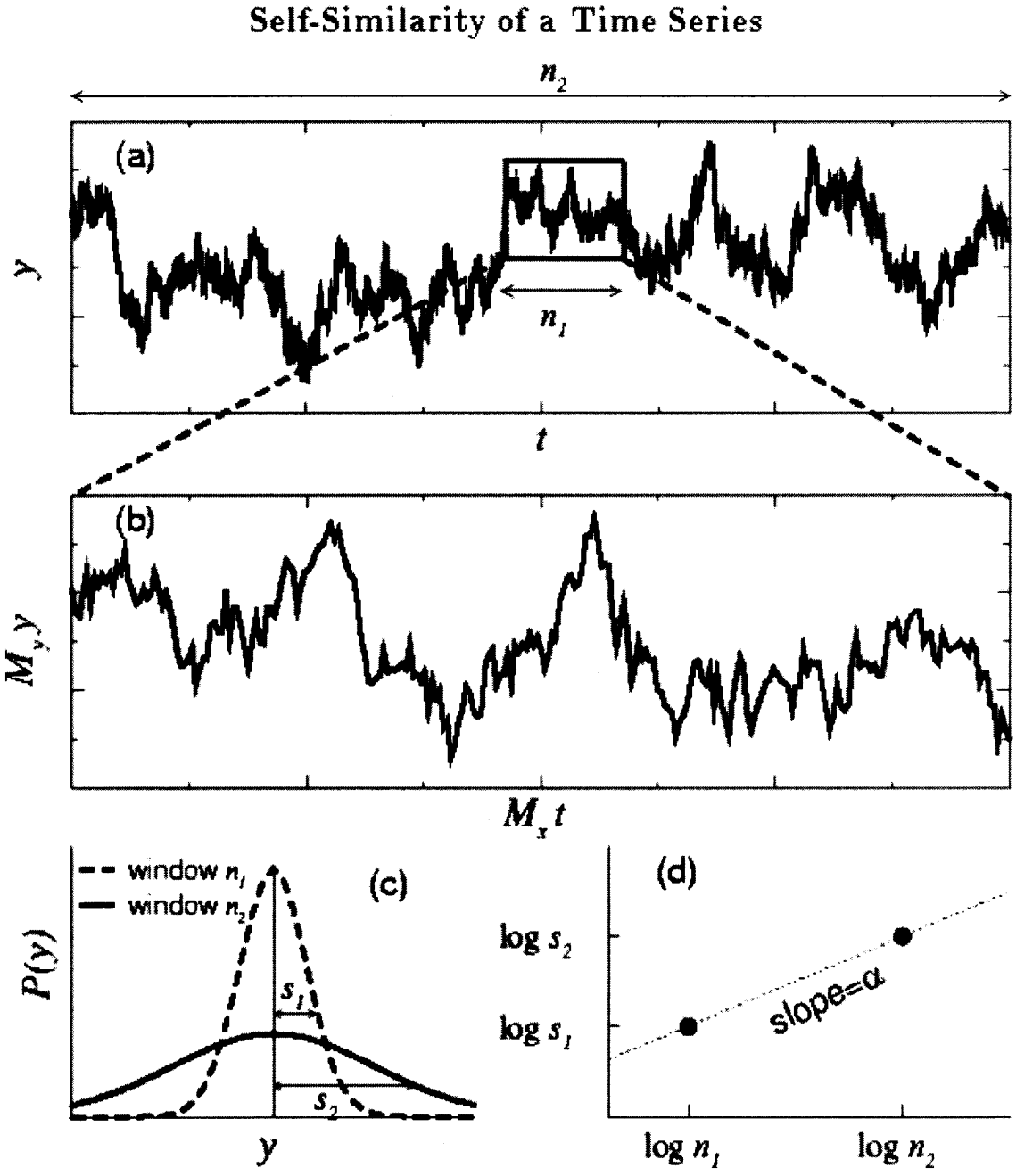

Figure 2.7 Illustration of the concept of self-similarity for a simulated random walk. (a) Two observation windows, with time scales n_1 and n_2, are shown for a self-similar time series $y(t)$. (b) Magnification of the smaller window with time scale n_1. Note that the fluctuations in (a) and (b) look similar provided that two different magnification factors, M_x and M_y, are applied on the horizontal and vertical scales, respectively. (c) The probability distribution, $P(y)$, of the variable y for the two windows in (a), where s_1 and s_2 indicate the standard deviations for these two distribution functions. (d) Log-log plot of the characteristic scales of fluctuations, s, versus the window sizes, n [15].

Figure 2.7(a) shows an example of a self-similar time series. By rescaling the x-axis and y-axis, one can get the time-series that is shown in Figure 2.7(b). The new rescaled time series resembles the original time series. The self-similarity parameter α defined in Equation 2.2 can be calculated by a simple relation

$$\alpha = \frac{\ln M_y}{\ln M_x} \tag{2.3}$$

where $M_x$and M_y are the appropriate magnification factors along the horizontal and vertical direction, respectively. We can calculate scaling exponent, α, by moving windows of different size in time series. This is explained in detail in Chapter 3.

It is important to know how the scaling attribute is calculated. From Figure 2.7, one can easily determine the magnification factors along the horizontal direction, $M_x = n_2/n_1$. But for the magnification factor along the vertical direction, M_y, we need to determine the vertical characteristic scales of windows 1 and 2. One way to do this is by examining the probability distributions (histograms) of the variable y for these two observation windows (Figure 2.7(c)). A reasonable estimate of the characteristic scales for the vertical heights, i.e., the typical fluctuations of y, can be defined by using the standard deviations of these two histograms, denoted as s_1 and s_2, respectively. Thus, we have $M_y = s_2/s_1$. Substituting M_x and M_y into Equation 2.3, we obtain

$$\alpha = \frac{\ln M_y}{\ln M_x} = \frac{\ln s_2 - \ln s_1}{\ln n_2 - \ln n_1} \tag{2.4}$$

In a time series, we perform the above calculations using the following procedures. For any given size of observation window, the time series is divided into subsets of independent windows of the same size. To obtain a more reliable estimation of the characteristic fluctuation at this window size, we average over all individual values of s obtained from these subsets and then we repeat these calculations, not just for two window sizes (as illustrated above), but for many different window sizes. The exponent α is estimated by fitting a line on the log-log plot of s versus n across the relevant range of scales because equetion 2.4 is nothing but the slope of two points (n_1,s_1) and (n_2,s_2) at log- log plot.

2.7.2 Mapping Real-world Time Series to Self-similar Processes

For a self-similar process with $\alpha > 0$, the fluctuations grow as the window size is increased. Therefore, the fluctuations of large observation windows are larger than those of smaller windows. As a result, the time series is unbounded. However, most physiologic time series are bounded as they cannot have arbitrarily large amplitudes. This can cause further complications for the analyses. Due to the bounded characteristic of the physiological time series, we do not need the rescaling of the y-axis. Thus, the y-axis scaling factor (M_y) is 0 as illustrated in Figure 2.7(a). Therefore, according to Equation 2.4, the self-similarity parameter (α) is 0 and no informative result can be obtained. Now, the main problem is how to distinguish the trivial parameter 0 in the case of uncorrelated noise, from the non-trivial parameter 0 computed for the original heart rate data.

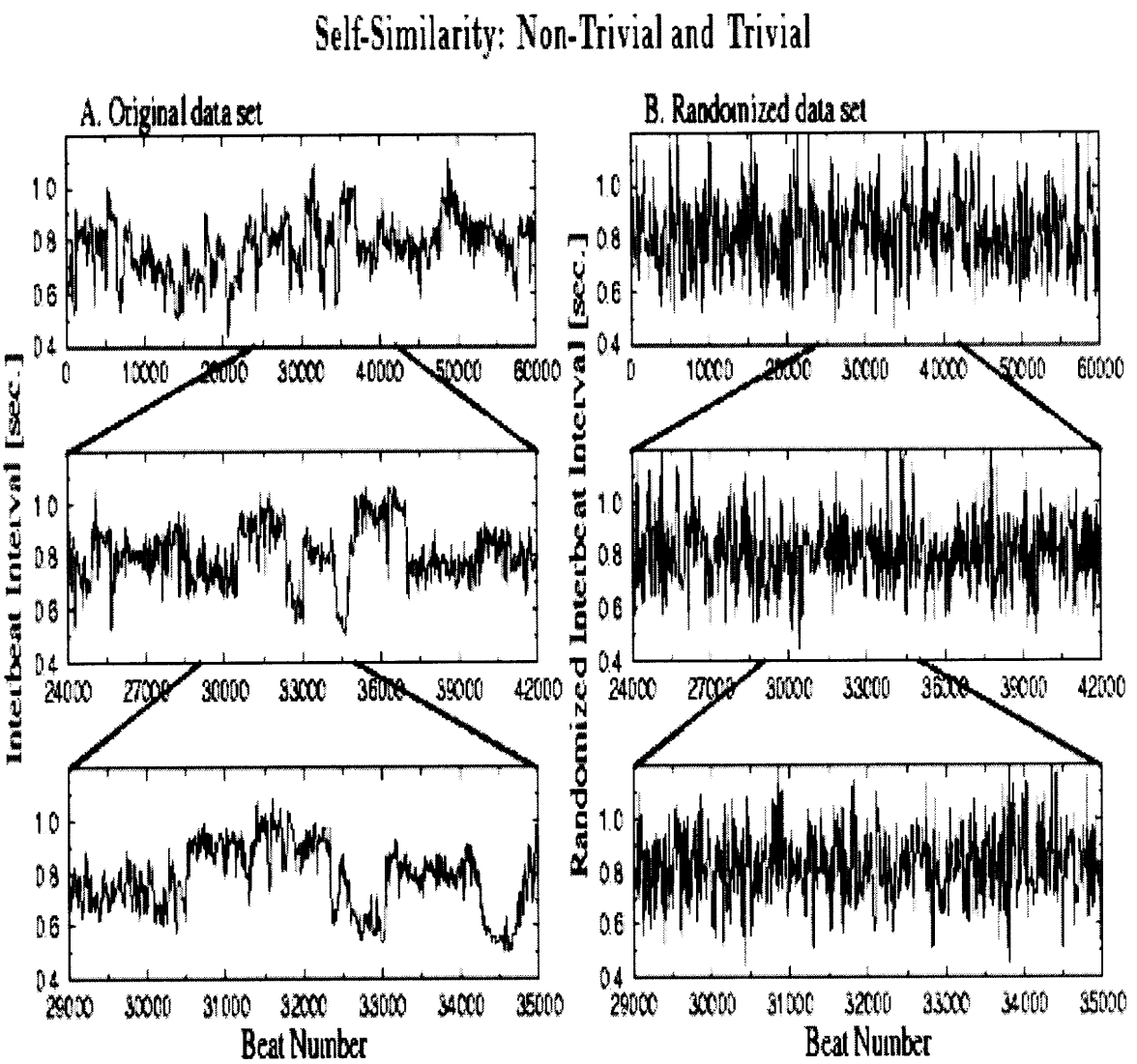

Figure 2.8 A cardiac inter-heartbeat interval (inverse of heart rate) time series is shown in (A) and a randomized control is shown in (B). Successive magnifications of the subsets show that both time series are self-similar with a trivial exponent $\alpha = 1$ (i.e., M_y=1), albeit the patterns are very different in (A) and (B).

The solution to this problem is the integration of the time series to study the fractal properties. One well-known physical example with relevance to biological time series is the dynamics of Brownian motion. In this case, the random force (noise) acting on particles is bounded, similar to physiologic time series. However, the trajectory (an integration of all previous forces) of the Brownian particle is not bounded and exhibits

fractal properties that can be quantified by a self-similarity parameter. When we apply fractal scaling analysis to the integrated time series of Figs. 2.8(A) and (B), the self-similarity parameters are indeed different in these two cases, providing meaningful distinctions between the original and the randomized control data sets. Mostly, integration of the original time series is applied for the fractal analysis of the signal.

While performing the analysis on the time series, one can find the complexity or non-complexity, regularity or non-regularity in the time series. The appearance of highly periodic dynamics and loss of complexity in the physiological signals are indication of the disease states in human. Complexity here refers specifically to a multiscale, fractal-type of variability in structure or function. Many disease states are marked by less complex dynamics than those observed under healthy conditions. This *de-complexification* of systems with disease appears to be a common feature of many pathologies, as well as of aging [16]. When physiologic systems become less complex, their information content is degraded. As a result, they are less adaptable and less able to cope with the exigencies of a constantly changing environment. To generate information, a system must be capable of behaving in an unpredictable fashion [15]. In contrast, a highly predictable, regular output is information-poor since it repeats its activity.

Quantitative assessment of periodic oscillations can be obtained by analyzing the time series of interest with a variety of standard techniques. It includes methods of linear dynamics and methods derived from non-linear dynamics as well. To a large extent, it is these periodicities and highly structured patterns -- the breakdown of multi-scale fractal complexity under pathologic conditions –that allow clinicians to identify and classify many pathologic features of their patients.

CHAPTER 3

MULTIFRACTAL ANALYSIS

Heart rate variability can be measured using various traditional (e.g., time domain, frequency domain) and nontraditional methods (e.g., 1/f spectral analysis, DFA, multifractal analysis). This Chapter provides information of different methods for HRV analysis and eventually concentrates on WTMM method (wavelet based method of multifractal analysis) of multifractal analysis. Methods of obtaining the HRV parameters are time domain methods, spectral domain methods and non - linear methods.

In time domain methods, the instantaneous heart rate is used or the intervals between successive R-R complexes are used. In a continuous electrocardiographic (ECG) record, each QRS complex is detected, and normal-to-normal (NN) intervals or RR intervals (i.e. intervals between adjacent QRS complexes), or the instantaneous heart rate is determined. The commonly used parameters used in the time domain include mean RR interval and mean heart rate. Time domain analysis assumes that the signal is stationary. Moreover, the main confusing factor in characterizing variability with standard deviation is the increase in baseline heart rate that may accompany diminished HRV indices. Another limitation of the time domain method, as explained in section 2.6, is that it does not distinguish between distinct biological signals by giving the same mean and standard deviation [17].

In the spectral domain method, collected physiological data is considered a sum of sinusoidal oscillations with distinct frequencies. Conversion from a time domain to frequency domain is performed by a Fourier transformation. The amplitude of each sine

and cosine wave determines its contribution to the biological signal; frequency domain analysis displays the contributions of each sine wave as a function of its frequency. Facilitated by computerized data harvest and computation, the result of converting data from time series to frequency analysis is termed spectral analysis because it provides an evaluation of the power (amplitude) of the contributing frequencies to the underlying signal. The important characteristics of the spectrum are the power of the spectrum and the powers of its separate zones. The following information is extracted from the physiological data. Measured parameters in this method are ULF (power in the ultra low frequency range; <0.003 Hz), VLF (power in the very low frequency range; 0.003 – 0.04 Hz), LF (power in the low frequency; 0.04 – 0.15 Hz) and HF (power in the high frequency range; 0.15 – 0.4 Hz). A recent review of HRV documented the evidence that ULF reflects changes secondary to the circadian rhythm, VLF is affected by temperature regulation and humoral systems, LF is sensitive to cardiac sympathetic and parasympathetic nerve activity, and HF is synchronized to respiratory rhythms, primarily related to vagal innervation. Moreover, the frequency values are the indication of the effect of the sympathetic and the parasympathetic activity on the heart.

There are some advantages and limitations to this method. In spectral domain analysis, it is assumed that the signal is stationary. It is the main disadvantage of this method. Spectral analysis is more sensitive to the presence of artifact than the time domain method. Moreover, level of activity, sleep pattern, change in posture can alter the LF and HF components of the spectral analysis [18].

We know that the heart is not a periodic oscillator under normal physiologic conditions and the commonly employed statistics of heart rate variability may not be able

to detect subtle, but important changes in the heart rate time series. Therefore several new analysis methods of heart rate behavior have been developed to quantify the dynamics of heart rate fluctuations based on nonlinear dynamics and chaos theory. As mentioned in the previous Chapter, the methods motivated by the nonlinear dynamics overcome some limitation that is faced in conventional time domain and power spectrum methods such as the assumption of the stationarity of the signals, periodicity and so forth.

The developed methods are approximate entropy, 1/f spectral analysis, detrended fluctuation analysis, multifractal analysis and so on. Now we will look into some of these methods and their terminologies, which are highly related to each other.

J.P.Saul et al.[31] used the spectral analysis technique to quantify the entire spectrum (0.00003-1.0 Hz) of HRV using a standard Holter monitor for 24hour ECG and found that the HRV contained 1/f behavior in the frequency range from 0.00003 to 0.1 Hz. A log-log plot of the power spectrum versus frequency shows that the power spectrum is inversely proportional to the frequency, 1/f. The log-log plot of the power spectrum S (f) vs. f is linear implies $S(f)=f^{-\beta}$.

The value of exponent $-\beta$ serves as an indicator of the health of the human. For the healthy subjects, value of β is approximately -1 ($\beta \approx -1$), which suggests the presence of the power law behavior in the time series [19]. Since the analysis of the power law behavior requires spectral analysis, the determination of the frequency components of the underlying signal, the technique becomes problematic when applied to nonstationary signals.

Approximate entropy (ApEn) provides a measure of irregularity and randomness within a series of data. ApEn was pioneered by Pincus as a measure of system

complexity [20]. In ApEn, smaller values indicate greater regularity, and greater values indicate more disorder, randomness and system complexity. Healthy human heart rate fluctuations are irregular so that one can say that the ApEn value is higher for healthy subjects and the value is lower for the diseased person. ApEn has been most extensively studied in the evaluation of heart rate dynamics. Heart rate becomes more orderly with age and in men, exhibiting decreased ApEn [21]. Heart rate ApEn has demonstrated the capacity to predict atrial arrhythmias, including spontaneous and postoperative atrial fibrillation after cardiac surgery, and to differentiate ventricular arrhythmias [20]. Heart rate ApEn is decreased in infants with aborted sudden infant death syndrome; among adults, postoperative patients with ventricular dysfunction and healthy individuals infused with endotoxin exhibit reduced heart rate ApEn [20]. ApEn statistics may be calculated for relatively short series of data, a principal advantage in their application to biological signals. Time series with 1000 or more data points can yield to the proper analysis of this method.

The detrended fluctuation analysis technique quantifies the presence or absence of fractal correlation properties. It was developed to characterize fluctuations on scales of all lengths. In DFA, the scaling exponent α is obtained using the DFA algorithm, which describes the fluctuation in the heart rate time series. One advantage of the DFA method is that it allows the detection of long-range power-law correlations in noisy signals with embedded polynomial trends that can mask the true correlations in the fluctuations of a signal. In DFA methods, it has been assumed that the value of the scaling exponent remains the same throughout the analysis. However, the empirical results show that the obtained value for α varies for small n (<10 beats) and larger n (>10 beats). The

presumption represents a somewhat arbitrary manipulation of the results of the analysis. The assumption that the same scaling pattern is present throughout the signal remains flawed, and therefore techniques without this assumption are being developed and are referred to as multifractal analysis.

3.1 Multifractal Analysis

DFA is a monofractal technique, in that the assumption is that the same scaling property is present throughout the entire signal. However, R-R interval time series have multiple scaling exponents. Multifractal techniques provide multiple, possibly infinite exponents, such that the analysis produces a spectrum rather than a discrete value of the exponents. For example, wavelet analysis is a multifractal analysis technique similar to DFA, which is capable of distinguishing the heart rate dynamics of patients with congestive heart failure from healthy control individuals [21].

3.2 Multifractal Formalism and Singularity

It was discussed that the heart rate signal is fractal. Recently, the approach towards fractals has been advanced to the *multifractal formalism*. The multifractal formalism is nothing but the statistical description of the scaling properties of a singularity or singular measures [26]. It is very interesting to acquire knowledge of a singularity in time series or in fractal signals because the heart rate dynamics are characterized by the singularities. The functions $f(t)$ typically studied in mathematical analysis are continuous and have

continuous derivatives. Hence, they can be approximated in the vicinity of some time t_i by a Taylor series or power series

$$f(t) = a_0 + a_1(t - t_i) + a_2(t - t_1)^2 + a_3(t - t_i)^3 + \dots . \quad (3.1)$$

For small regions around t_i, just a few terms of the expansion Equation 3.1 are necessary to approximate the function *f(t)*. Most of the time series *f(t)* found in real-life applications are noisy (Fig. 3.1). Therefore, they cannot be approximated by Taylor series of just a few terms. Moreover, many experimental or empirical time series have fractal features--i.e., for some times t_i, the series *f(t)* displays singular behavior. That is, at those times t_i, the signal has components with non-integer powers of time which appear as step-like or cusp-like features, the so-called singularities, in the signal. Figure 3.1 illustrates step like (blue color) and cusp like(green color) singularities.

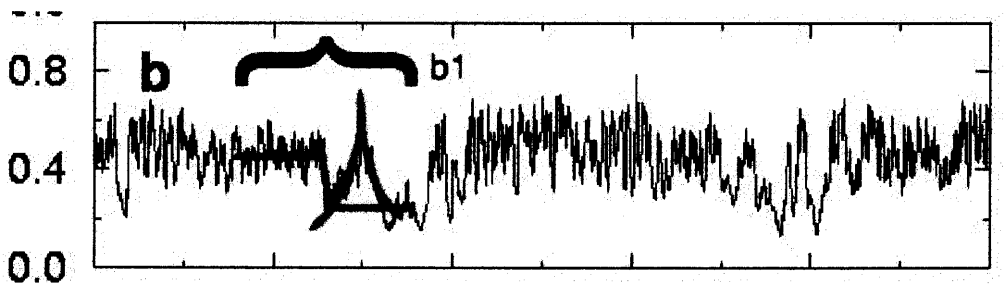

Figure 3.1 Time series with singularities [23].

Formally one can write:

$$f(t) = a_0 + a_1(t - t_i) + a_2(t - t_1)^2 + a_3(t - t_i)^3 + \dots + a_h(t - t_i)^{h_i}, \quad (3.2)$$

where t is inside a small vicinity of t_i, and h_i is a non-integer number quantifying the local singularity of *f(t)* at $t = t_i$ [22].

The multifractal signals show multi-singularity behavior meaning that fractal objects or signals can be decomposed into interwoven sets which are characterized by their singularity strength-α and their Hausdorff dimension-f(α) (measurement of fractal dimension). The Hausdorff dimension by itself measures the singularity in the function *f(t)* by finding the non-integer dimension of fractals.

The Hausdorff dimension can measure the dimension of the fractals. The Hausdorff dimension- *d* of a set is defined as $H^d(f)$. Suppose one take a non-fractal object that has the Hausdorff (s=1)-measure as shown in figure 3.2. *Measure* is a function that allows us to compare sizes of sets.

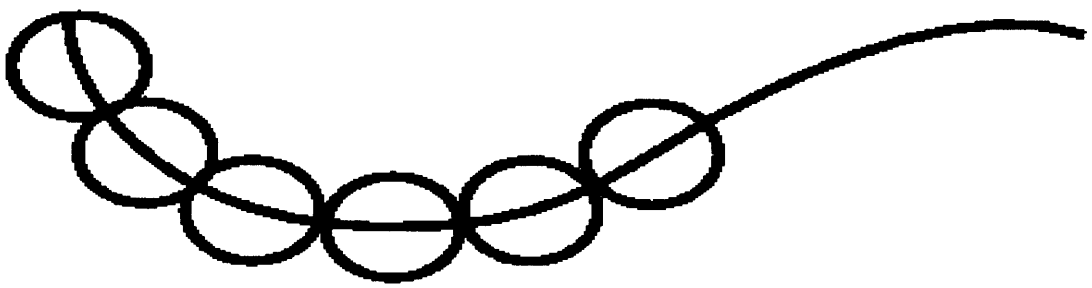

Figure 3.2 Curve filled with balls [24].

If selected non-fractal object, *f*, is covered with epsilon (ball that has almost zero radius) balls in very organized way, and add up the lengths, one can see a polygonal approximation to *f*. So as epsilon goes to zero, we must get that $H^1(f) = L(f)$, the length of the curve *f*. We see in fact, that for a given epsilon, we need approximately L(f)/Є little balls, so $H^1(f)=\lim_{\varepsilon\to 0}(L(f)/\varepsilon)\varepsilon^1=L(f)$.

If we calculate the same curve-*f* with Hausdorff 2-measure, we will not get the Length of that curve. Following is the mathematical presentation

$H^2(f)=\lim_{\varepsilon\to 0}(L(f)/\varepsilon)\varepsilon^2=\lim_{\varepsilon\to 0}L(f)\varepsilon=0$

Similarly, if we take the Hausdorff 2-measure of a square or other nice Euclidean planar figure, we get something that gives area, whereas 3-measure gives 0 and 1 measure gives infinity. Thus, the Hausdorff measure behaves in a way that makes sense on sets that we are familiar with. Now the dimension s is not only an integer, in fact, it can be any real number. If we consider any given set F, it turns out that there is a unique d such that the following holds:

$$\begin{aligned} \text{if } s < d,\ \mathcal{H}^s(F) &= \infty \\ \text{if } s > d,\ \mathcal{H}^s(F) &= 0 \end{aligned} \qquad (3.3)$$

We call this d the *fractal dimension* of the set F. We call F a fractal if the fractal dimension is strictly greater than another quantity known as the *topological dimension* [24]. Now one can write the singularity spectrum as follow:

$$f(\alpha) = \dim_H\{x|\ \mu(B_x(\epsilon)) \sim \epsilon^{\alpha}, \text{ for } \epsilon \to 0\} \qquad (3.4)$$

where $B_x(\epsilon)$ is the ϵ size box at point x and μ is the measure and α represent the singularity value or singularity strength. The $f(\alpha)$ spectrum is the humped shape curve over a finite interval $[\alpha_{min}, \alpha_{max}]$ where α_{min} represents strongest singularities whereas, α_{max} represents weakest singularities.

The statistical properties of the different subsets characterized by these different noninteger exponents h_i can be quantified by the function D(h) where $D(h_0)$ is also the fractal dimension of the subset of the time series and gives an alternate way to measure singularities.

The Wavelet transform using the Wavelet transform Maxima Modulus method (wavelet based method of multifractal analysis to detect singularities in the signal) is very efficient to provide thermodynamics of multifractal distributions. Moreover, it provides

efficient way to detect singularities. To understand the WTMM method, it is better to understand the wavelet transform first.

3.3 The Wavelet Transform

Until recently, the Fourier transform was the main tool to analyze singularities. The Fourier transform provides overall description of the regularity of signals. It does not provide exact location of the singularities in the time series. However, the Wavelet transform overcomes this problem. It decomposes the signal into elementary building blocks, which are well localized both in space and frequency. Furthermore, it helps to detect a singularity at the exact location in the time series. Moreover, it can characterize the local regularity of signals. The wavelet transform (WT) decomposes function f into its elementary space-scale plane, associated to the so-called *wavelets,* which are constructed from one single function, the analyzing wavelet Ψ, by mean of translations and dilations. The WT of f is defined as:

$$W_{\psi}[t](b,a) = \frac{1}{a}\int_{-\infty}^{+\infty} \overline{\psi}\left(\frac{t-b}{a}\right) f(t)\,dt \qquad (3.5)$$

where a $\in R^{+*}$ is a scale parameter, b $\in$ R is a space parameter and Ψ is the complex conjugate of Ψ. The analyzing wavelet Ψ is generally chosen to be well localized in both space and frequency [35]. Usually, Ψ is required to have zero mean but, for the particular purpose of singularity tracking, we will require Ψ to be orthogonal to some low-order polynomials:

$$\int_{-\infty}^{+\infty} t^m \psi(t)\,dt = 0, \qquad \forall m, \quad 0 \le m < n_\psi \tag{3.6}$$

There are almost as many analyzing wavelets as applications of the WT. A class of commonly used real-valued analyzing wavelets which satisfies the above condition is given by the successive derivatives of the Gaussian function:

$$\psi^{(N)}(t) = \frac{d^N}{dt^N} e^{-t^2/2} \tag{3.7}$$

Here, the higher the order, N, of the derivative, the higher the order of the polynomial trends removed and the better the detection of the temporal structure of the local scaling exponents in the signal [27]. One determines the coefficients of the wavelet transform by convolving *f(t)* with a *Gaussian function.*

As mentioned before, the wavelet transform easily removes polynomial contributions that would mask singular (fractal) behavior. To illustrate this fact, consider a signal *f(t)* that one can expand for t close to t_i as a series of the form of Equation 3.2. In a fractal analysis, one wants to measure h_i, but for small values of $t - t_i$, the trend $(t - t_i)^k$ with $k < h_i$ will dominate the sum. Hence, one wants to remove all terms $(t - t_i)^k$ for which $k < h_i$ in order to get the singularity value. By convolving *f(t)* with an appropriate wavelet function, one can put to zero all coefficients that would arise from such polynomial contributions. For instance, the derivative of order k of the Gaussian convolves to zero all polynomial terms up to order $k - 1$. Thus, detection of singularities becomes very easy with the use of the Gaussian function [33].

3.4 Singularity Detection Using Wavelets

The strength of the singularity of a function is defined by an exponent called- the Holder exponent. The Holder exponent of a function *f* at some point t_0 is defined as follows:

$$|f(t) - P_n(t-t_0)| \leq C|t - t_0|^h \tag{3.8}$$

where, $h(t_0)$ is a holder exponent of given function *f* at point t0. $h(t_0)$ is the largest exponent such that there exists a polynomial $P_n(t)$ [25]. Here, t is in the neighborhood of t_0 and *f* is n times differentiable at the point t_0. One can easily prove that *f* is n times but not n + 1 times differentiable at the point t_0. The polynomial *Pn(t)* corresponds to the Taylor series of s around $t = t_0$, up to the order n [29]. Thus, *h(to)* measures how irregular the function *f* is at the point t_0. The higher the exponent *h(to),* the more regular the function *f.* This definition of the singularity strength naturally leads to a generalization of the $f(\alpha)$ singularity spectrum introduced for fractal measures. Henceforth, we will denote *D(h)* the Hausdorff dimension of the set where the Holder exponent is equal to h meaning :

$$D(h) = dH\{t, h(t) = h\} \tag{3.9}$$

Where *d* stands for dimension. If one uses an analyzing wavelet Ψ, that satisfies the Equation 3.8, the local behavior of *f* in Equation 3.10 is mirrored by the wavelet transform, which locally behaves like:

$$W_\psi[f](t_0, a) \sim a^{h(t_0)} \tag{3.10}$$

in the limit a $\rightarrow 0^+$. Therefore, one can extract the exponent *h(to)* from a log-log plot of the WT amplitude versus the scale a. Moreover, if $n_\Psi < h(to)$, one could prove that we would still get a power law behavior but with a scaling exponent n_Ψ:

$$W_\Psi[f](t_0,a) \sim a^{n\Psi} \tag{3.11}$$

3.4 Singularity Detection Using Wavelets

The strength of the singularity of a function is defined by an exponent called- the Holder exponent. The Holder exponent of a function *f* at some point t_0 is defined as follows:

$$|f(t) - P_n(t-t_0)| \leq C|t - t_0|^h \tag{3.8}$$

where, $h(t_0)$ is a holder exponent of given function *f* at point t0. $h(t_0)$ is the largest exponent such that there exists a polynomial $P_n(t)$ [25]. Here, t is in the neighborhood of t_0 and *f* is n times differentiable at the point t_0. One can easily prove that *f* is n times but not n + 1 times differentiable at the point t_0. The polynomial *Pn(t)* corresponds to the Taylor series of s around $t = t_0$, up to the order n [29]. Thus, *h(to)* measures how irregular the function *f* is at the point t_0. The higher the exponent *h(to),* the more regular the function *f.* This definition of the singularity strength naturally leads to a generalization of the $f(\alpha)$ singularity spectrum introduced for fractal measures. Henceforth, we will denote *D(h)* the Hausdorff dimension of the set where the Holder exponent is equal to h meaning :

$$D(h) = dH\{t, h(t) = h\} \tag{3.9}$$

Where *d* stands for dimension. If one uses an analyzing wavelet Ψ, that satisfies the Equation 3.8, the local behavior of *f* in Equation 3.10 is mirrored by the wavelet transform, which locally behaves like:

$$W_\psi[f](t_0, a) \sim a^{h(t_0)} \tag{3.10}$$

in the limit a $\rightarrow 0^+$. Therefore, one can extract the exponent *h(to)* from a log-log plot of the WT amplitude versus the scale a. Moreover, if $n_\Psi < h(to)$, one could prove that we would still get a power law behavior but with a scaling exponent n_Ψ:

$$W_\Psi[f](t_0,a) \sim a^{n\Psi} \tag{3.11}$$

Thus, around a given point t_0, the faster the wavelet transform decreases when the scale a goes to zero, the more regular *f* is around that point.

3.5 The Wavelet Transform Modulus Maxima Method (WTMM)

When investigating a fractal function, locally, the Holder exponent $h(t_0)$ is governed by the Singularities, which accumulate at t_0. This results in unavoidable oscillations around the expected power-law behavior of the WT amplitude so we cannot calculate exactly the value of h by taking a log plot of Equation (3.13). The WTMM method overcome this exact calculation problem.

In order to understand the wavelet transform modulus maxima method, we have to be familiar with modulus maximum and maxima line. Following are the definition of modulus maximum, and maxima line [29].

- We call modulus maximum, any point (a_o, *t,)* such that $|Wf(a_0, t)| < |Wf(a_0, t_0)|$ when t belongs to either a right or the left neighborhood of t_0,, and $|Wf(a_0,t)| <= |Wf(a_0, t_0)|$ when t belongs to the other side of the neighborhood of t_0.
- We call maxima line, any connected curve in the scale space (a, t*)* along which all points are modulus maxima.

Now a function is not singular in any neighborhood where its wavelet transform has no modulus maxima at fine scales. So, one can find the singularity by following the value of the maxima line.

The other fundamental advantage of using wavelets is that the *wavelet transform modulus-maxima* provides an adaptive space-scale partition to extract the *D(h),* singularity spectrum, via the scaling behavior of some partition functions defined on the

WTMM. In the WTMM method, we are concerned about the values of $\tau(q)$ and D(h). The *partition function* is used to find the values of $\tau(q)$, which evaluates the multifractality of the signal. Partition function, Z, is an important quantity that encodes the statistical properties of a system and relates it with some variable (in our case $\tau(q)$). The partition function Z(q,a), in WTMM, is defined as the sum of the q^{th} power of the local maxima of the modulus of the wavelet transform coefficients at scale *a*.

$$Z(q,a) = \sum_{\ell \in \mathcal{L}(a)} \left(\sup_{(t,a') \in \ell} |W_\psi[t](t,a')|^q \right) \tag{3.12}$$

In Equation 3.12, *l* is a maxima line and *L(a)* is a set of maxima lines at scale *a*. In the presence of singularities in data, power law behavior is observed for the partition function.

$$Z(q,a) \sim a^{\tau(q)} \tag{3.13}$$

Thus, $\tau(q)$ is obtained with the use of the partition function. For positive q values, *Z*(q,a) is calculated for the larger fluctuation and strong singularities in the signal at each scale. On the other hand, for negative q values, Z(q,a) finds $\tau(q)$ values for the smaller fluctuation and weak singularities in the signal at each scale. Once the $\tau(q)$ value is retrieved, then the singularity spectrum can be calculated using the Legendre transform (method of changing the dependence of a function of one set of variables to another set of variables).

$$D(h) = qh - \tau(q) \tag{3.14}$$

The obtained singularity and $\tau(q)$ spectrum reveals aspects of the cardiac dynamics. For example, for healthy subjects, the D(h) spectrum is non-zero in a broad

range and $\tau(q)$ is nonlinear, whereas the D(h) spectrum is narrow and the $\tau(q)$ spectrum is relatively linear for the subjects with congestive heart failure.

3.6 $\tau(q)$ and D(h) Spectrum of the Predefined Time Series

In this section, multifractal analysis has been performed on some synthetic time series using the multifractal analysis program available on PhysioNet. Linear and nonlinear aspects have been checked on random, periodic, monofractal and multifractal signals.

All mentioned signals are generated in MATLAB, except the binomial time series, with 40000 data points. For the random signal, random numbers have been generated between –1 to 1. A periodic signal is generated using sine functions. Fractional Brownian motion is a random walk that has a defined h value of $0 < h < 1$ [31]. Fractional Brownian motion has been generated by integrating the random number time series. The fractional Brownian motion time series is a monofractal time series. The last signal used for the multifractal analysis is a binomial time series, which is a multifractal time series. The binomial time series is used to check multifractal behavior of the signal. Figures 3.3, 3.4, 3.5 and 3.6 are periodic, random, monofractal (fractional brownian motion) and multifractal (binomial time series) series respectively. Figures 3.7 and 3.8 show the $\tau(q)$ and the D(h) spectrum of the mentioned signals, respectively. Multifractal binomial time series gives the nonlinear $\tau(q)$ spectrum, whereas monofractal fractional Brownian motion gives linear spectrum and so do periodic and random time series. For binomial time series, the D(h) spectrum has values of D(h) in broad range of h values, while values of D(h) are in narrower range of h for fractional Brownian motion.

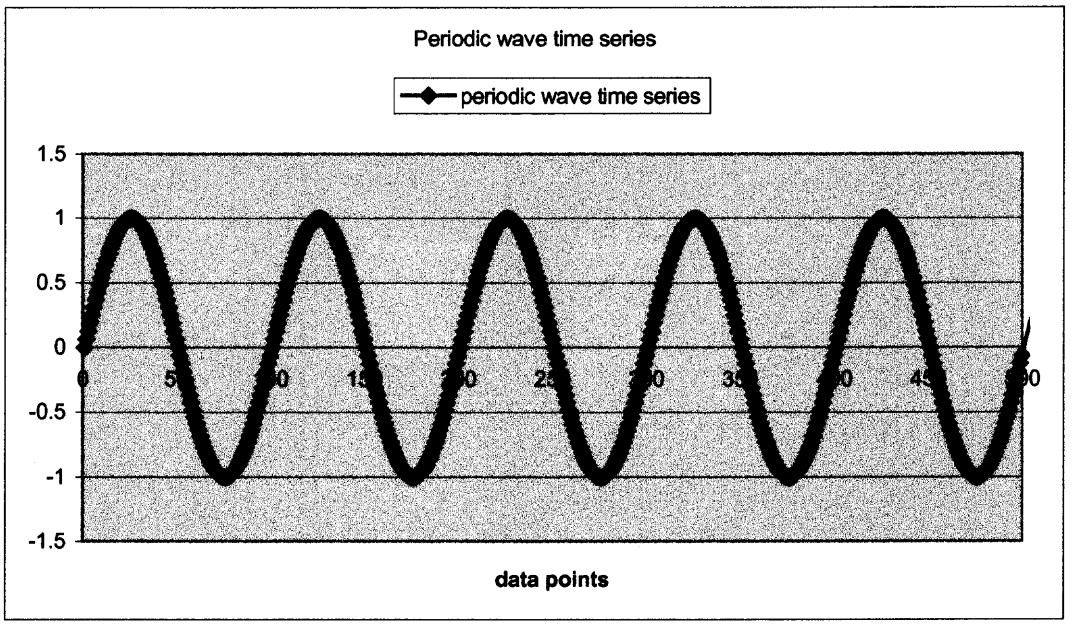

Figure 3.3 A periodic signal.

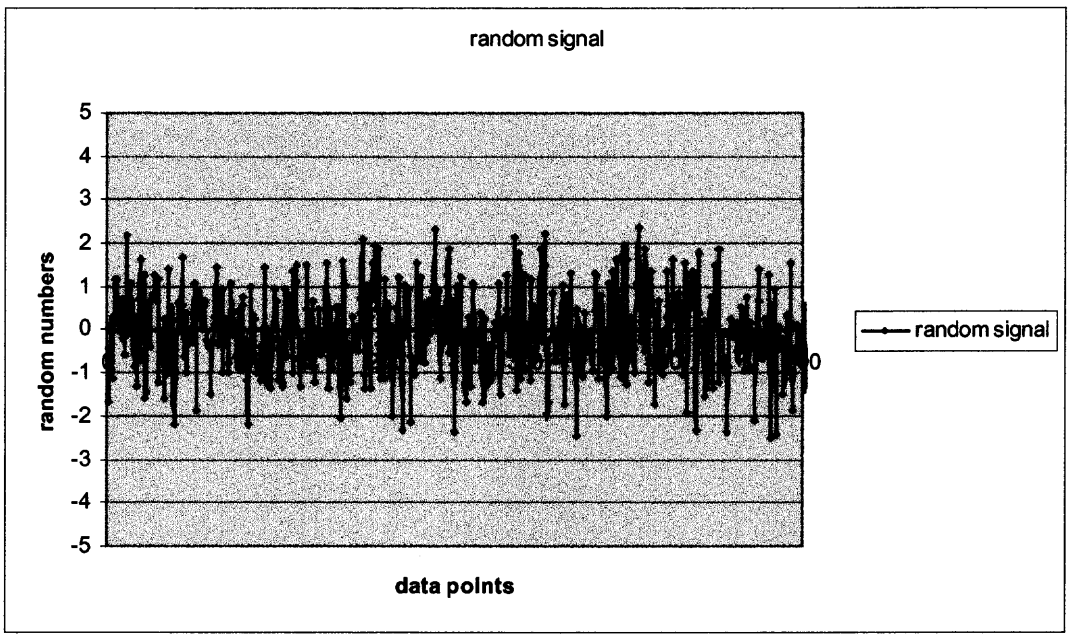

Figure 3.4 A random signal

Figures 3.7 and 3.8 shows the multifractal spectrum and the singularity spectrum for the artificially generated different mentioned time series.

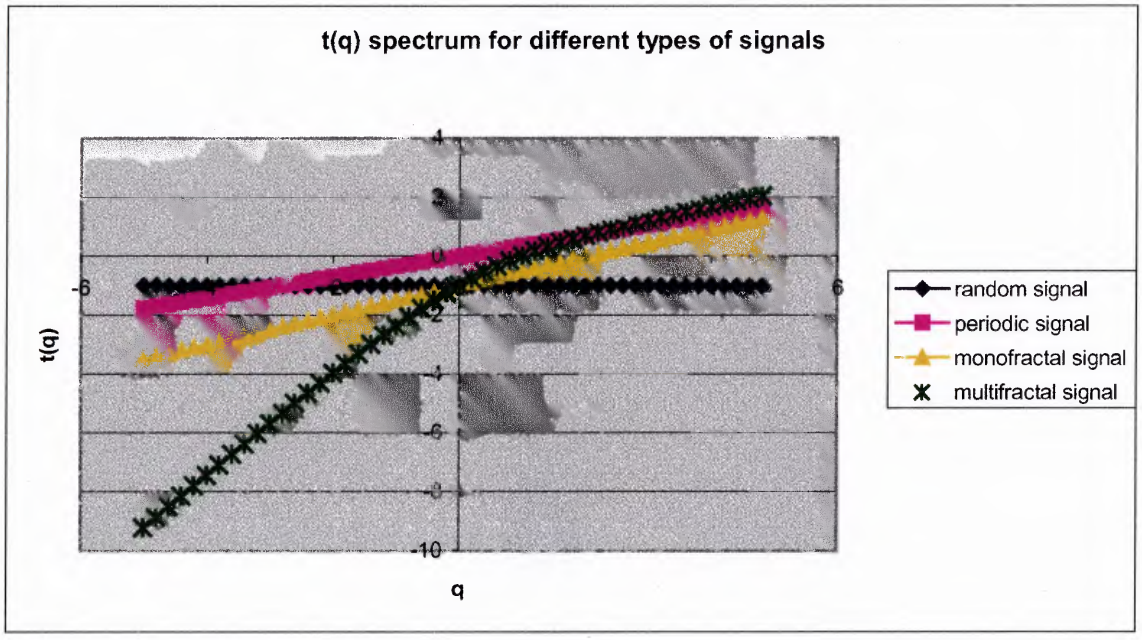

Figure 3.7 Comparison of the τ(q) spectrum of periodic signal, random signal, monofractal brownian signal and multifractal binomial signal.

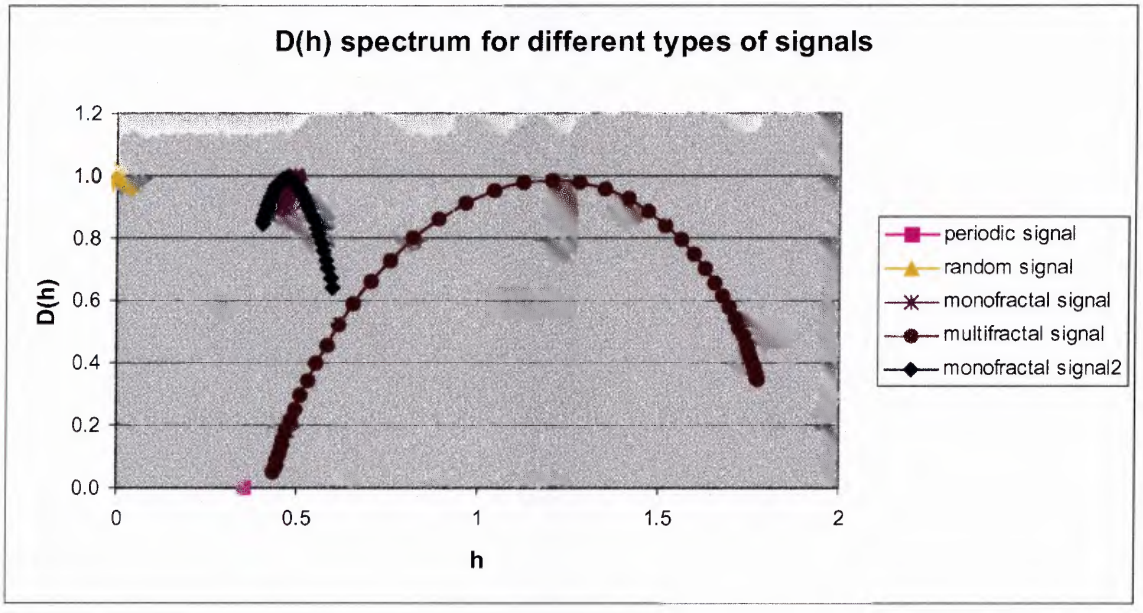

Figure 3.8 Comparison of the D(h) spectrum of periodic signal, random signal, monofractal brownian signal and multifractal binomial signal.

Figures 3.7 and 3.8 shows the multifractal spectrum and the singularity spectrum for the artificially generated different mentioned time series.

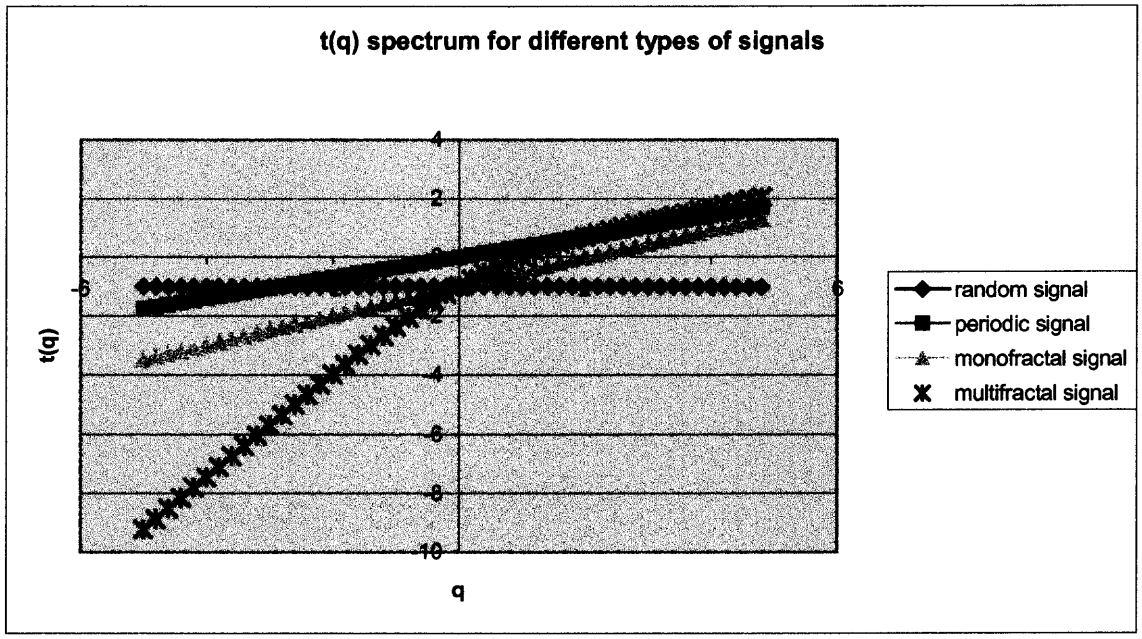

Figure 3.7 Comparison of the $\tau(q)$ spectrum of periodic signal, random signal, monofractal brownian signal and multifractal binomial signal.

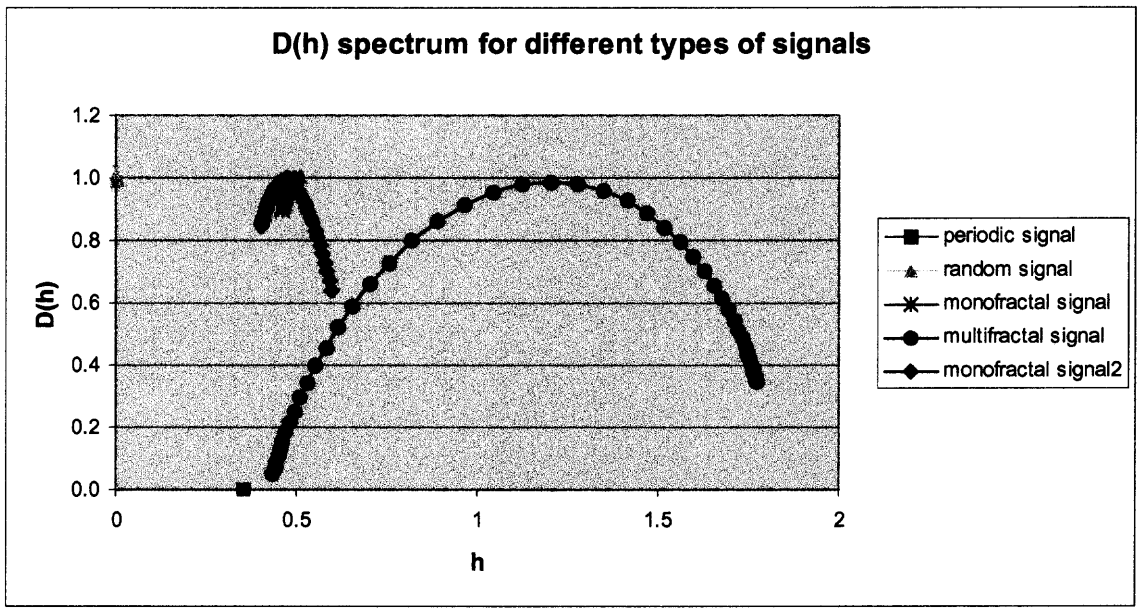

Figure 3.8 Comparison of the D(h) spectrum of periodic signal, random signal, monofractal brownian signal and multifractal binomial signal.

3.7 Algorithm

The algorithm is available on PhysioNet and written in C language. The software package contains two files: Multifractal.c and mf_moments_lt.awk.

The multifractal.c calculates the multifractal partition functions of a time series. The program output is obtained in three different formats [25]:

- It is a text file in which the first column is the scale and remaining columns gives the partition functions for all different moments-q in selected range (range is specified during the execution of the multifractal program). Output values are log1-transformed.
- It is in text format that contains maxima lines. The first column is the index of the time series (time index), and the second is the scale where the maximum appears at that time. The scales are log10-transformed.
- (PPM image, wavelet cascade) This file can be viewed using the freely available display application included in ImageMagick, as well as a variety of other image viewers.

The $\tau(q)$ and multifractal spectrum D(h) of the input time series can be obtained from the partition functions using mf_moments_lt.awk program.

The multifractal.c program finds the wavelet convolution of the signal for increasing wavelet scale and locates the local maxima of the absolute value of the wavelet coefficient as a function of time for each wavelet scale. Afterwards, the program checks whether a local maximum at a given wavelet scale is located close to a maximum at a smaller scale or not- if yes then connect both maxima and generate the maxima lines, otherwise cancel it. The program also checks that the number of maxima at larger scales is less or equal to that at a smaller scale and track maxima lines for increasing wavelet scale and that basically helps to detect the singularity as explained in the theory. The Multifractal program generates the multifractal partition function, using the command:

multifractal INPUT N QMIN QMAX DW MODE >OUTPUT

where, INPUT name of file containing the input time series

N number of points (lines) in INPUT

QMIN minimum order of moment, q

QMAX maximum order of moment, q

DW order of the Gaussian derivative wavelet (0-7)

MODE the type of output to be produced, one of:

1. partition functions (text)
2. maxima lines (text)
3. wavelet cascade (PPM image)

After obtaining the partition function (OUTPUT FILE from the execution of the multifractal program), we may calculate the $\tau(q)$ spectrum and the multifractal spectrum D(h), using the awk program, mf_moments_lt.awk:

```
awk -f mf_moments_lt.awk -v a=1 -v b=2.53 OUTPUT >out.tq
```

The parameters a and b are the upper and lower limits of the scaling range. The program reads OUTPUT(the output file that we have just obtained from multifractal), and it writes the corresponding $\tau(q)$ and D(h) curves into out.tq file.

CHAPTER 4

DATA ACQUISITION AND ANALYSIS

4.1 Data Acquisition

The number of data points required for the multifractal analysis is 30000. RR interval time series is given as an input in the multifractal analysis code. The RR interval time series data with desired (minimum six hours) data length is available on the www.physionet.org website. The data for the normal control group were obtained from 24 hr. Holter monitor recordings of 35 subjects from the PhysioNet normal sinus rhythm database with ECG data sampled at 128 Hz. Data were acquired from the men and women of age 20-76 years. The data for the congestive heart failure (CHF) group were obtained from 24 hours Holter monitor recordings of 25 subjects from the PhysioNet CHF database with ECG data sampled at 250 Hz. The obtained RR time series data directly from the normal control group and CHF group were unformatted for the multifractal analysis program. The "ann2rr" program, written in MATLAB, was used to convert unformatted data to the proper text format. The "ann2rr" program is also available on the PhysioNet. The multifractality of the heart rate signal is not affected by the activities of a subject. The multifractal analysis on sleep stage data (nighttime) and daytime data were performed and compared to validate the effect of sleep. The data were obtained from two subjects (two men aged 21-26 years) using the Polar S810 Heart Rate Monitor. The monitor records the RR interval. The seven hours of data were obtained during the sleep stage from all two subjects between 12 a.m. to 7 a.m. and seven hours of data were obtained during daytime without doing any activity between 9 a.m. to 4 p.m.

Data for the sleep stage during nighttime and for the awake stage (without doing any activity) were obtained on the same day for a particular subject.

4.2 Data Correction

Obtained data from the PhysioNet website contained some undesired RR interval entries called outliers. These outliers show major effect in the output of the multifractal analysis. Entries of the outliers were removed using the "deglitching" code available on the PhysioNet. The code, written in MATLAB, removes the outliers by comparing the data set with an Auto Regressive prediction model of order three. If the data point is within 25% to 75% of the predicted value, then the point is labeled valid, otherwise invalid. Only valid points are used for the multifractal analysis purpose.

4.3 System Requirements and Data Analysis

The Multifractal analysis program is available on www.physionet.org/physiotools/multifractal. As mentioned before, code for the multifractal analysis is written in C language. The software package contains two main files: multifractal.c and mf_moments_lt.awk. The obtained software requires Unix, Linux, Mac OS X systems, or Cygwin to execute the software files. Redhat Linux 9.0 is used for the data analysis. In order to compile and execute the program, the system requires:

- A C compiler (gcc is recommended)

- awk (or gawk) pattern scanning and processing language
- make (optional but recommended)

The C compiler is used to compile multifractal.c file and awk or gawk is used to compile and run mf_momentjs_lt.awk file. The *make* file contains a list of the commands that can be executed simultaneously. The input file to run the multifractal.c is a text file containing two columns of numbers; the first is number of the data point, and the second contains the data values.

One can type *make check* to compile and test the software. If one is not using the make utility, *gcc -o multifractal -O multifractal.c –lm* is required to be typed on the command window of the Linux based system. *gcc -o multifractal -O multifractal.c –lm* command basically compile ibs.c and link it with the C standard math library. The executed line with the gcc command simply makes an executable file called *multifractal.* This executable file (*multifractal*) has to be typed on the command prompt to run our multifractal.c program. The mf_moments_lt.awk file is automatically executed when we type *awk* command on the command prompt.

4.4 Results

This section will display the results of the multifractal analysis method obtained on the normal subjects data and the data of the subjects with CHF. The effect of the different data length and activity on the multifractal analysis has been shown. Moreover, results of two different data sets(normal subjects data and the data of subjects with CHF) have been compared.

Table 4.1 indicates D(h) vs. h values for different order of Gaussian derivative (Gaussian derivative 1, 2, 3, 4, 5 and 7, respectively) for NSR group. Figure 4.1 is the D(h) spectrum from the values in Table 4.1. In the same way, Table 4.2 indicates D(h) vs. h values for different orders of Gaussian derivative for the CHF group. Figure 4.2 shows the spectrum of D(h) from the values in Table 4.2. Mean h and mean D(h) values are taken from the ten randomly selected NSR subjects and ten randomly selected CHF subjects at each different Gaussian derivative.

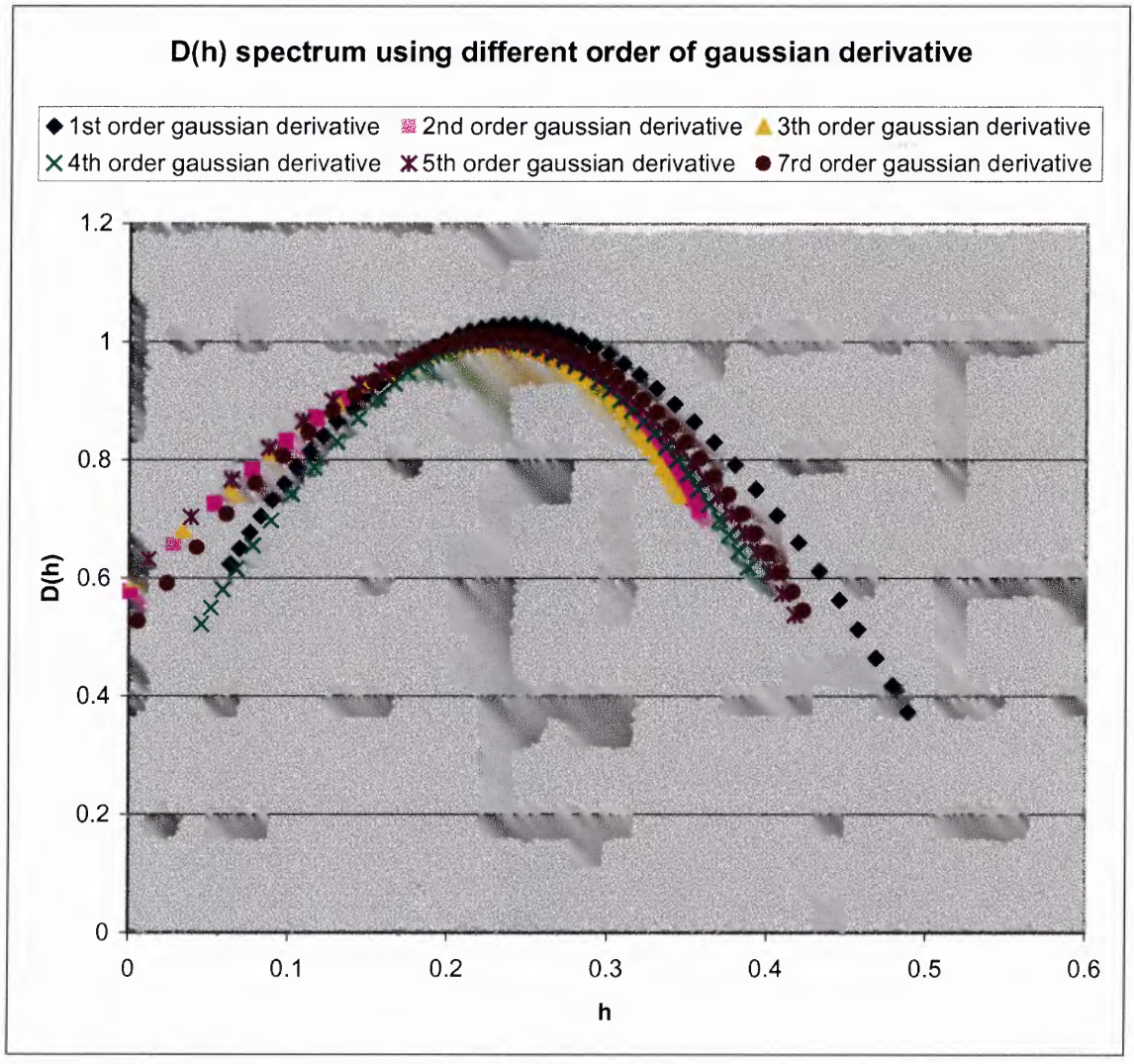

Figure 4.1 D(h) vs. h for different values of Gaussian derivative for NSR group.

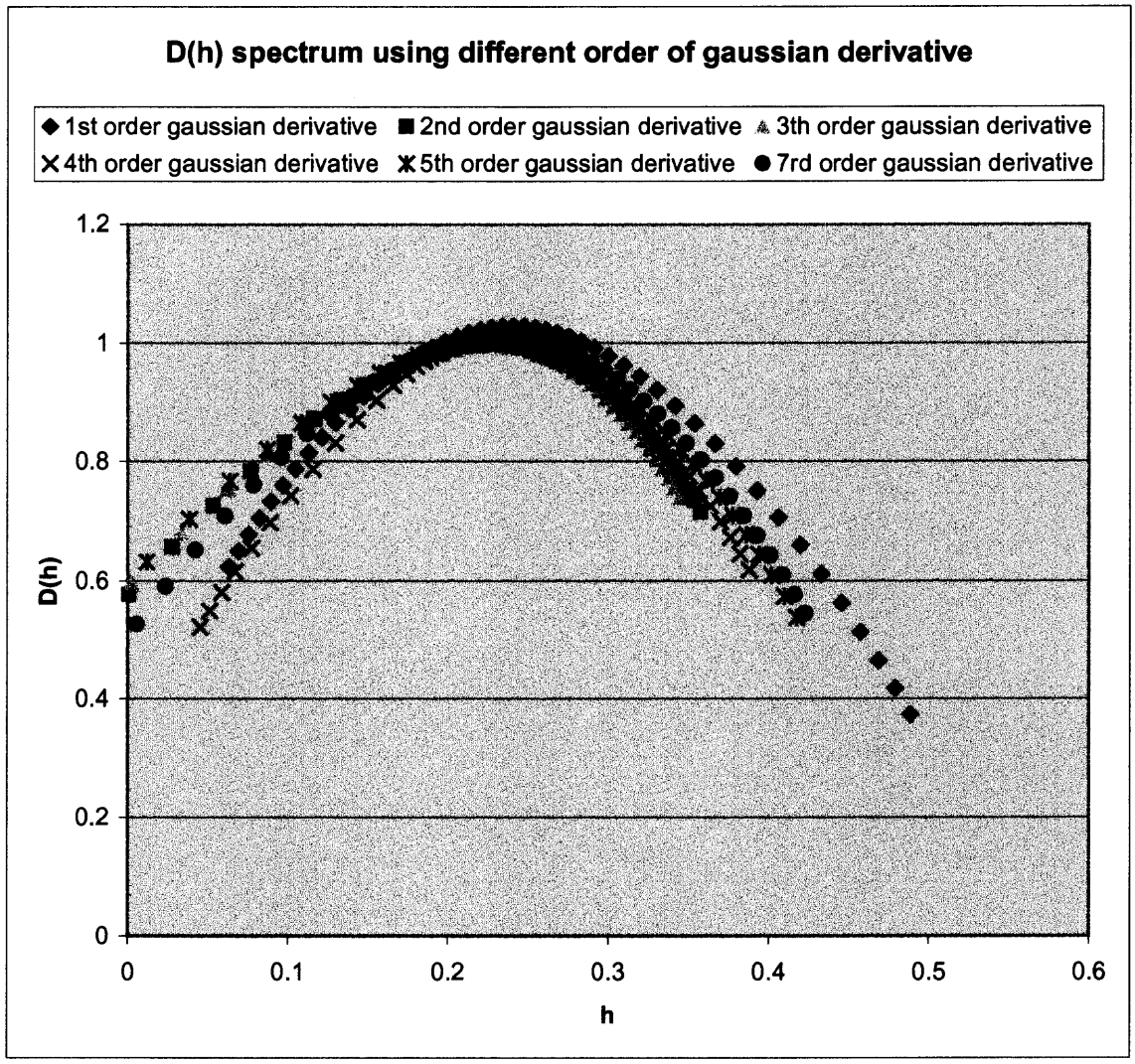

Figure 4.1 D(h) vs. h for different values of Gaussian derivative for NSR group.

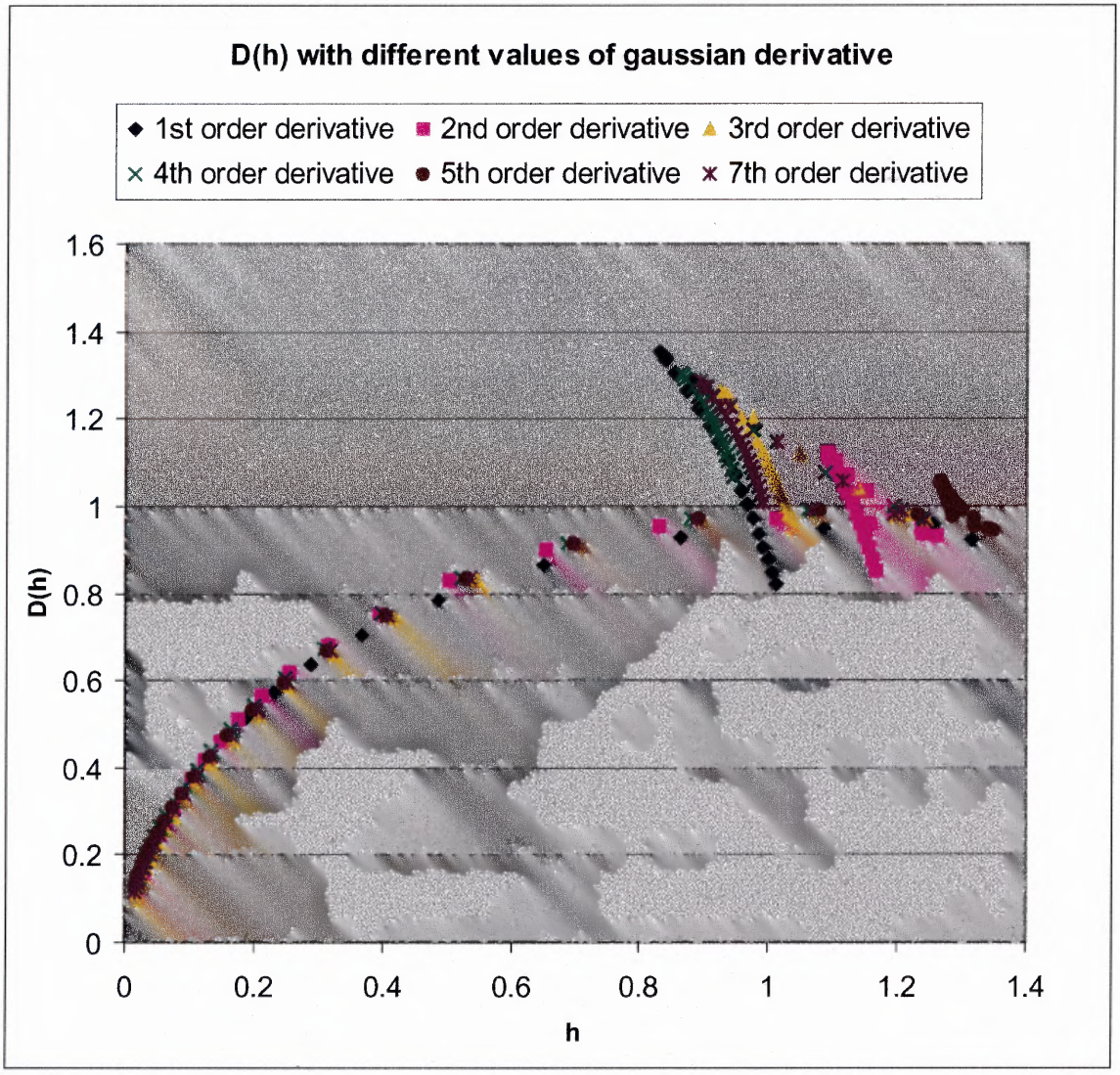

Figure 4.2 D(h) vs. h for different values of Gaussian derivative for CHF group.

Table 4.3 shows the effect of length on $\tau(q)$ for 10K-30K data points. To investigate the minimum data set requirement, analysis has been performed separately on 10K to 90K data points for NSR group.

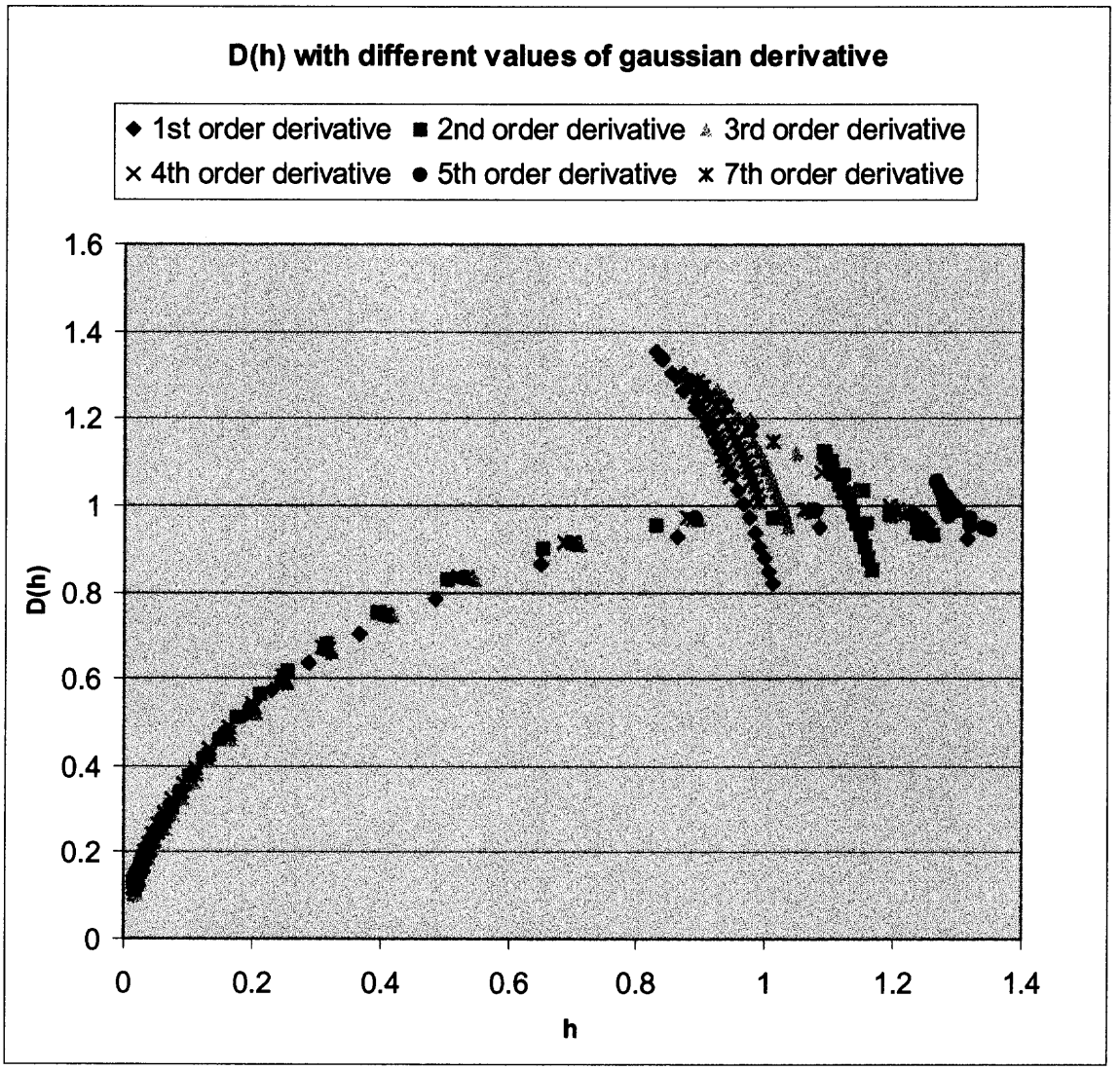

Figure 4.2 D(h) vs. h for different values of Gaussian derivative for CHF group.

Table 4.3 shows the effect of length on $\tau(q)$ for 10K-30K data points. To investigate the minimum data set requirement, analysis has been performed separately on 10K to 90K data points for NSR group.

Table 4.3 Effect of Data Length (10K, 20K and 30K) on τ(q) for the NSR Group.

Data length	10K	20K	30K
Q			
-5.0	-3.333440	-3.098190	-2.857460
-4.8	-3.174770	-2.958550	-2.749070
-4.6	-3.018430	-2.822870	-2.641770
-4.4	-2.864930	-2.691580	-2.535750
-4.2	-2.714860	-2.565050	-2.431270
-4.0	-2.568920	-2.443660	-2.328610
-3.8	-2.427840	-2.327710	-2.228070
-3.6	-2.292430	-2.217400	-2.129990
-3.4	-2.163440	-2.112890	-2.034710
-3.2	-2.041620	-2.014190	-1.942590
-3.0	-1.927570	-1.921250	-1.853960
-2.8	-1.821740	-1.833910	-1.769140
-2.6	-1.724350	-1.751930	-1.688370
-2.4	-1.635400	-1.675000	-1.611870
-2.2	-1.554650	-1.602780	-1.539750
-2.0	-1.481640	-1.534880	-1.472050
-1.8	-1.415780	-1.470930	-1.408720
-1.6	-1.356340	-1.410500	-1.349660
-1.4	-1.302550	-1.353210	-1.294690
-1.2	-1.253610	-1.298670	-1.243590
-1.0	-1.208750	-1.246510	-1.196110
-0.8	-1.167240	-1.196350	-1.151990
-0.6	-1.128420	-1.147840	-1.110970
-0.4	-1.091680	-1.100640	-1.072810
-0.2	-1.056500	-1.054420	-1.037250
0.0	-1.022410	-1.008890	-1.004080
0.2	-0.989030	-0.963756	-0.973080
0.4	-0.956040	-0.918786	-0.944070
0.6	-0.923200	-0.873768	-0.916860
0.8	-0.890340	-0.828541	-0.891290
1.0	-0.857340	-0.783001	-0.867210
1.2	-0.824170	-0.737076	-0.844470
1.4	-0.790820	-0.690766	-0.822940
1.6	-0.757350	-0.644112	-0.802490
1.8	-0.723830	-0.597203	-0.783020
2.0	-0.690400	-0.550167	-0.764420
2.2	-0.657170	-0.503162	-0.746600
2.4	-0.624280	-0.456368	-0.729480
2.6	-0.591890	-0.409974	-0.713000
2.8	-0.560110	-0.364173	-0.697100
3.0	-0.529080	-0.319151	-0.681750
3.2	-0.498910	-0.275080	-0.666910
3.4	-0.469680	-0.232112	-0.652560
3.6	-0.441480	-0.190377	-0.638700
3.8	-0.414360	-0.149979	-0.625340
4.0	-0.388370	-0.110995	-0.612470
4.2	-0.363520	-0.073475	-0.600110
4.4	-0.339830	-0.037448	-0.588270
4.6	-0.317300	-0.002914	-0.576980
4.8	-0.295910	0.030139	-0.566250

Figures 4.3, 4.4 and 4.5 are graphical presentations of the τ(q) spectrum for Table 4.3 values for 10K, 20K and 30K respectively, while Figure 4.6 shows the comparison of the τ(q) spectrum for 10K, 20K and 30K data points.

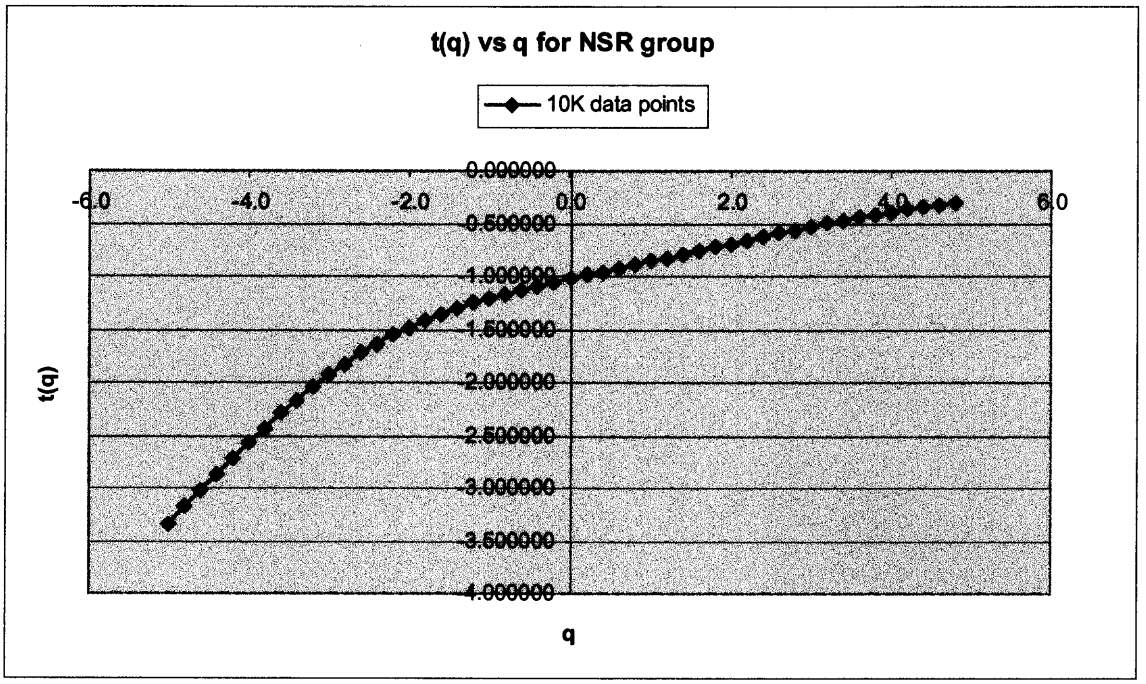

Figure 4.3 τ(q) spectrum for 10K data points for NSR group.

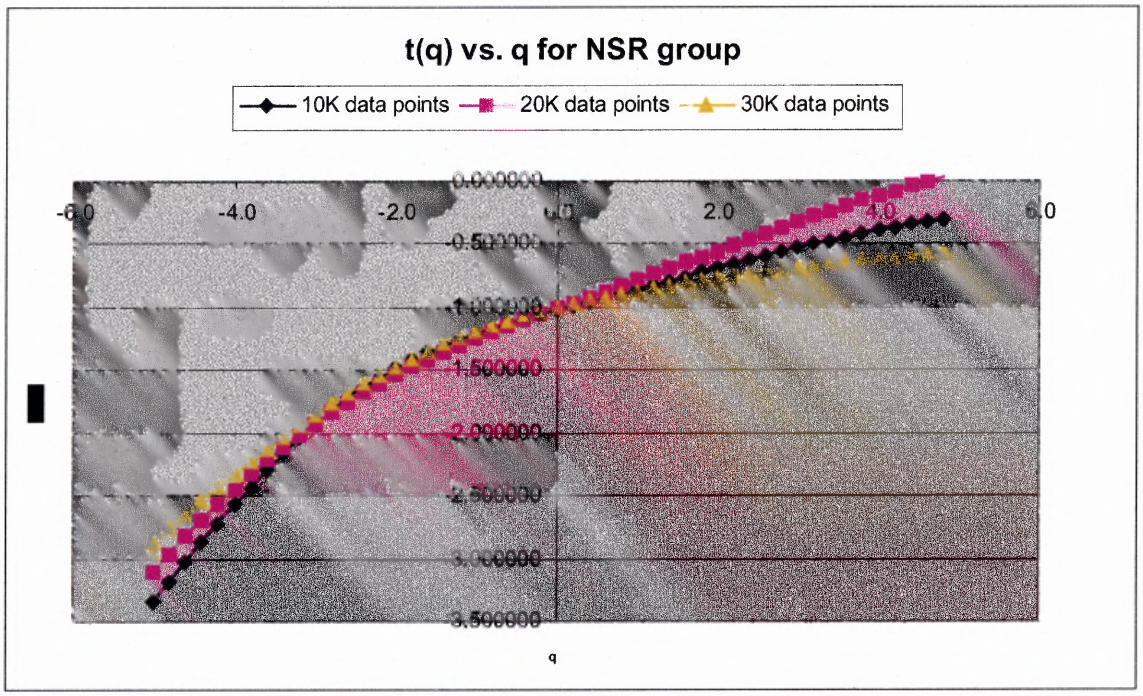

Figure 4.6 Comparison of τ(q) spectrum for 10K, 20K and 30K data points for NSR group.

Table 4.4 shows the effect of length on τ(q) for 30K to 90K data points for NSR group. Again, to investigate the minimum data set requirement, analysis has been performed separately on 10K to 30K data points and 30K to 90K data points for NSR group. Table 4.5 shows the effect of length on τ(q) for 30K to 90K data points for CHF group. Figure 4.7 is graphical illustration of the τ(q) spectrum for NSR group and Figure 4.8 is graphical illustration of the τ(q) spectrum for the CHF group. Total 30 subjects (15 from CHF group and 15 from NSR group) were randomly selected and mean value at each moment resolution was calculated.

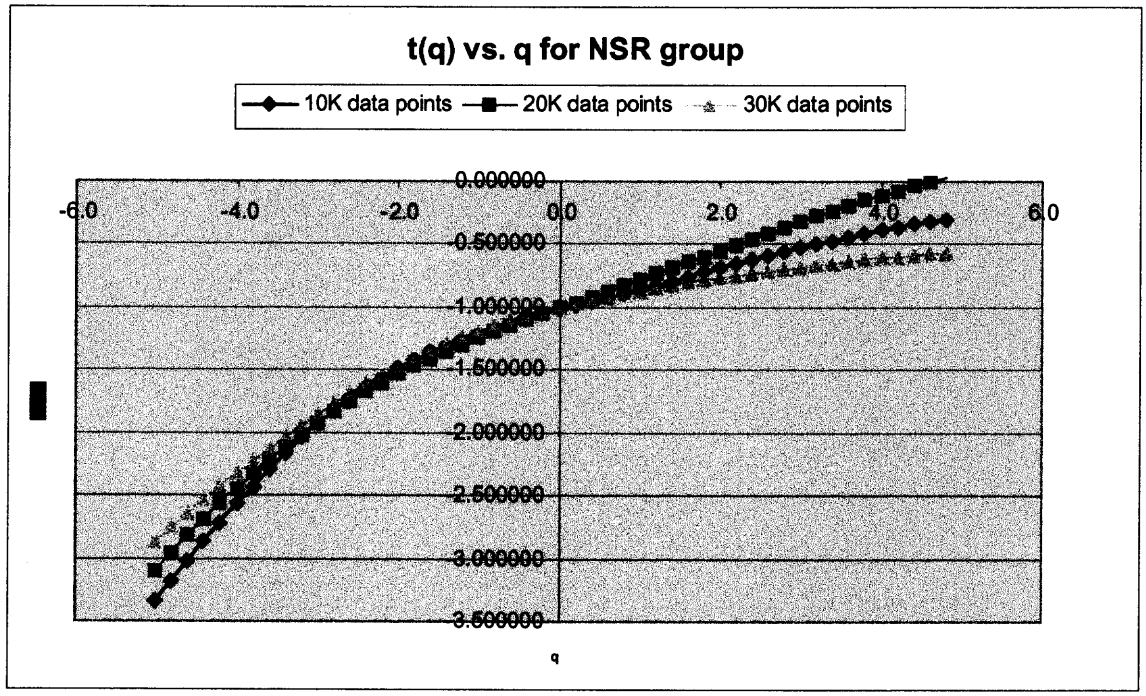

Figure 4.6 Comparison of $\tau(q)$ spectrum for 10K, 20K and 30K data points for NSR group.

Table 4.4 shows the effect of length on $\tau(q)$ for 30K to 90K data points for NSR group. Again, to investigate the minimum data set requirement, analysis has been performed separately on 10K to 30K data points and 30K to 90K data points for NSR group. Table 4.5 shows the effect of length on $\tau(q)$ for 30K to 90K data points for CHF group. Figure 4.7 is graphical illustration of the $\tau(q)$ spectrum for NSR group and Figure 4.8 is graphical illustration of the $\tau(q)$ spectrum for the CHF group. Total 30 subjects (15 from CHF group and 15 from NSR group) were randomly selected and mean value at each moment resolution was calculated.

Table 4.4 Effect of Data Length (30K to 90K) on $\tau(q)$ for NSR Group.

Data length	30K	40K	50K	60K	70K	80K	90K	Var
q								
-5	-2.85746	-2.81967	-2.79186	-2.64850	-2.54299	-2.54163	-2.54199	0.02024
-4.8	-2.74907	-2.70925	-2.68058	-2.54418	-2.44471	-2.44335	-2.44368	0.01866
-4.6	-2.64177	-2.59983	-2.57033	-2.44110	-2.34793	-2.34661	-2.34687	0.01709
-4.4	-2.53575	-2.49167	-2.46136	-2.33956	-2.25295	-2.25168	-2.25191	0.01553
-4.2	-2.43127	-2.38506	-2.35402	-2.23988	-2.16008	-2.15892	-2.15908	0.01399
-4	-2.32861	-2.28035	-2.24864	-2.14241	-2.06967	-2.06867	-2.06876	0.01247
-3.8	-2.22807	-2.17790	-2.14564	-2.04754	-1.98206	-1.98131	-1.98133	0.01098
-3.6	-2.12999	-2.07812	-2.04544	-1.95568	-1.89763	-1.89720	-1.89715	0.00954
-3.4	-2.03471	-1.98144	-1.94851	-1.86722	-1.81671	-1.81668	-1.81657	0.00817
-3.2	-1.94259	-1.88828	-1.85530	-1.78255	-1.73959	-1.74006	-1.73990	0.00687
-3	-1.85396	-1.79908	-1.76627	-1.70201	-1.66652	-1.66757	-1.66740	0.00568
-2.8	-1.76914	-1.71420	-1.68183	-1.62590	-1.59766	-1.59938	-1.59922	0.00460
-2.6	-1.68837	-1.63396	-1.60231	-1.55442	-1.53311	-1.53555	-1.53545	0.00365
-2.4	-1.61187	-1.55861	-1.52798	-1.48770	-1.47285	-1.47605	-1.47606	0.00283
-2.2	-1.53975	-1.48829	-1.45898	-1.42576	-1.41680	-1.42076	-1.42092	0.00215
-2	-1.47205	-1.42304	-1.39535	-1.36855	-1.36480	-1.36950	-1.36984	0.00160
-1.8	-1.40872	-1.36279	-1.33700	-1.31592	-1.31661	-1.32198	-1.32255	0.00117
-1.6	-1.34966	-1.30739	-1.28376	-1.26766	-1.27197	-1.27792	-1.27871	0.00083
-1.4	-1.29469	-1.25661	-1.23539	-1.22350	-1.23060	-1.23697	-1.23796	0.00058
-1.2	-1.24359	-1.21017	-1.19156	-1.18316	-1.19218	-1.19879	-1.19994	0.00039
-1	-1.19611	-1.16775	-1.15194	-1.14634	-1.15643	-1.16305	-1.16427	0.00026
-0.8	-1.15199	-1.12904	-1.11616	-1.11273	-1.12306	-1.12941	-1.13057	0.00016
-0.6	-1.11097	-1.09370	-1.08387	-1.08204	-1.09180	-1.09757	-1.09848	0.00010
-0.4	-1.07281	-1.06142	-1.05472	-1.05400	-1.06241	-1.06725	-1.06767	0.00005
-0.2	-1.03725	-1.03189	-1.02839	-1.02836	-1.03469	-1.03822	-1.03784	0.00002
0	-1.00408	-1.00485	-1.00458	-1.00488	-1.00843	-1.01026	-1.00873	0.00001
0.2	-0.97308	-0.98003	-0.98301	-0.98336	-0.98348	-0.98323	-0.98012	0.00001
0.4	-0.94407	-0.95719	-0.96342	-0.96360	-0.95972	-0.95700	-0.95186	0.00005
0.6	-0.91686	-0.93613	-0.94559	-0.94547	-0.93707	-0.93152	-0.92385	0.00011
0.8	-0.89129	-0.91664	-0.92934	-0.92882	-0.91547	-0.90678	-0.89607	0.00022
1	-0.86721	-0.89854	-0.91450	-0.91354	-0.89491	-0.88282	-0.86858	0.00038
1.2	-0.84447	-0.88167	-0.90094	-0.89955	-0.87541	-0.85974	-0.84148	0.00059
1.4	-0.82294	-0.86588	-0.88858	-0.88681	-0.85705	-0.83766	-0.81490	0.00086
1.6	-0.80249	-0.85105	-0.87736	-0.87528	-0.83992	-0.81673	-0.78903	0.00120
1.8	-0.78302	-0.83705	-0.86728	-0.86500	-0.82418	-0.79712	-0.76406	0.00160
2	-0.76442	-0.82380	-0.85838	-0.85599	-0.80997	-0.77898	-0.74014	0.00206
2.2	-0.74660	-0.81119	-0.85073	-0.84834	-0.79749	-0.76245	-0.71742	0.00258
2.4	-0.72948	-0.79918	-0.84446	-0.84217	-0.78693	-0.74765	-0.69602	0.00318
2.6	-0.71300	-0.78770	-0.83972	-0.83759	-0.77847	-0.73466	-0.67600	0.00385
2.8	-0.69710	-0.77671	-0.83666	-0.83477	-0.77230	-0.72352	-0.65740	0.00461
3	-0.68175	-0.76619	-0.83547	-0.83386	-0.76856	-0.71423	-0.64021	0.00549
3.2	-0.66691	-0.75611	-0.83629	-0.83501	-0.76736	-0.70676	-0.62440	0.00652
3.4	-0.65256	-0.74647	-0.83926	-0.83832	-0.76877	-0.70104	-0.60993	0.00773
3.6	-0.63870	-0.73725	-0.84446	-0.84388	-0.77281	-0.69698	-0.59673	0.00918
3.8	-0.62534	-0.72846	-0.85194	-0.85172	-0.77942	-0.69448	-0.58473	0.01091
4	-0.61247	-0.72009	-0.86168	-0.86183	-0.78853	-0.69340	-0.57385	0.01296
4.2	-0.60011	-0.71216	-0.87362	-0.87413	-0.79999	-0.69363	-0.56401	0.01539
4.4	-0.58827	-0.70467	-0.88764	-0.88852	-0.81365	-0.69503	-0.55514	0.01824
4.6	-0.57698	-0.69762	-0.90362	-0.90485	-0.82932	-0.69746	-0.54718	0.02154
4.8	-0.56625	-0.69102	-0.92140	-0.92297	-0.84681	-0.70081	-0.54004	0.02532

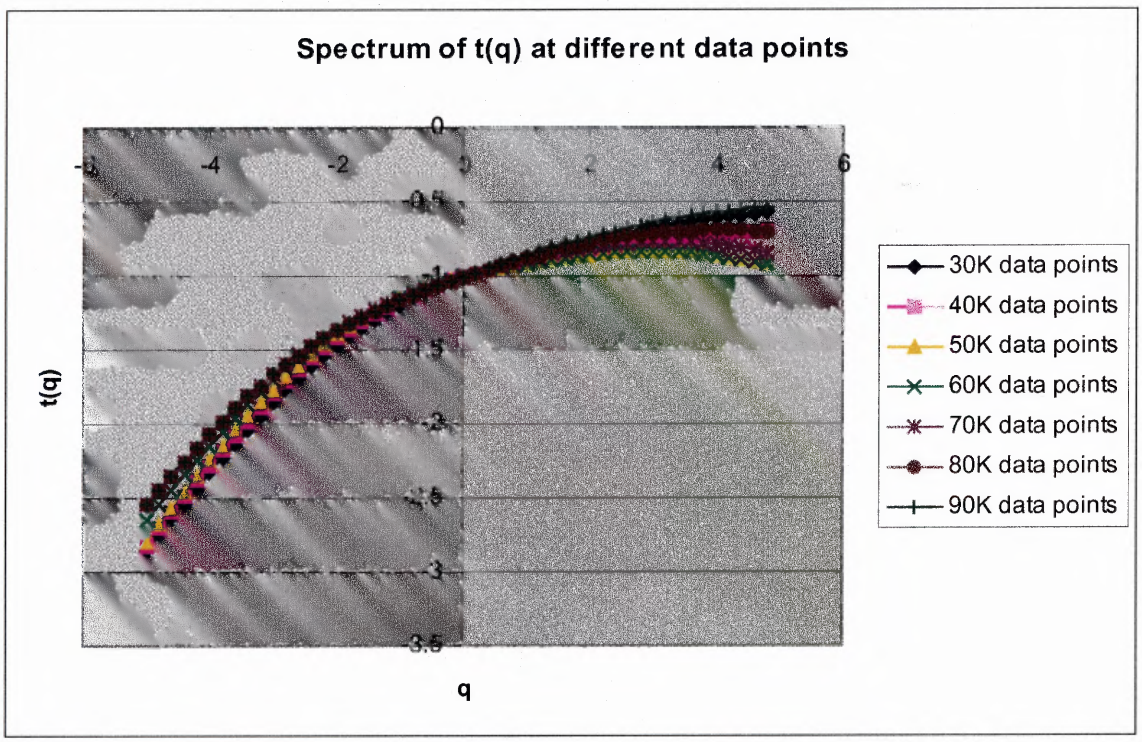

Figure 4.7 Effect of data-length on τ(q) for 30K to 90K data points with the increase of 10K data points for NSR group.

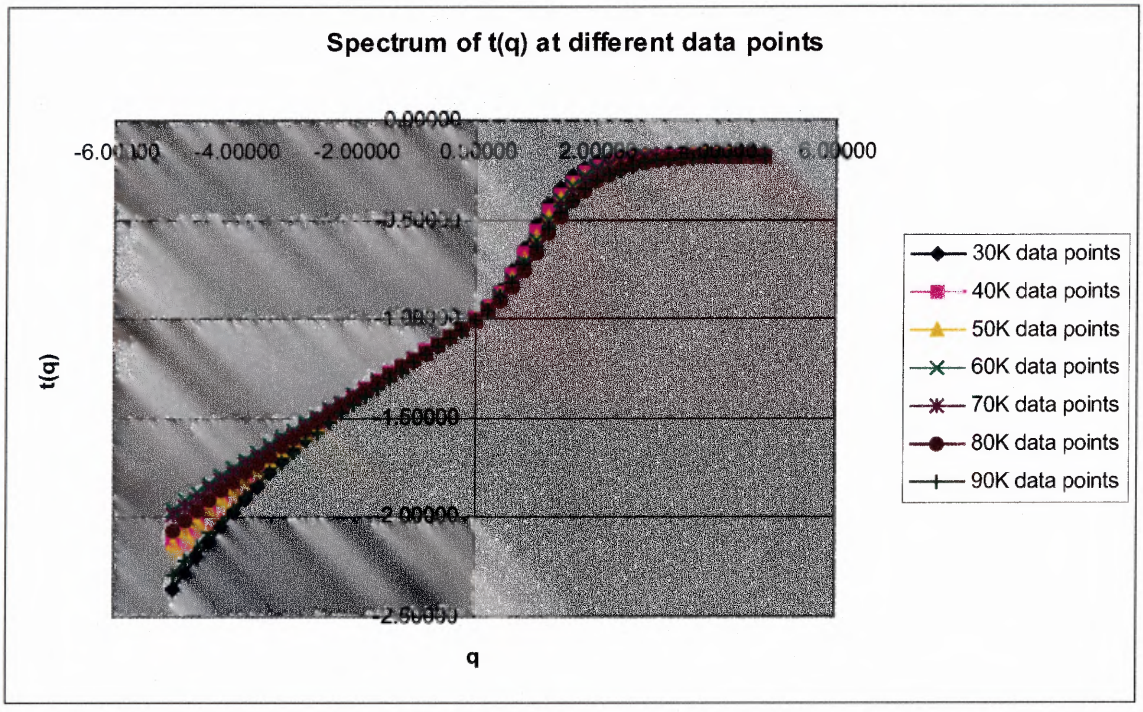

Figure 4.8 Effect of data-length on τ(q) for 30K to 90K data points with the increase of 10K data points for CHF group.

Table 4.6 shows mean τ(q) values for 25 CHF subjects and 25 NSR subjects. Figure 4.9 is τ(q) spectrum drawn from Table 4.6. The shape of the τ(q) spectrum is used to differentiate between two groups.

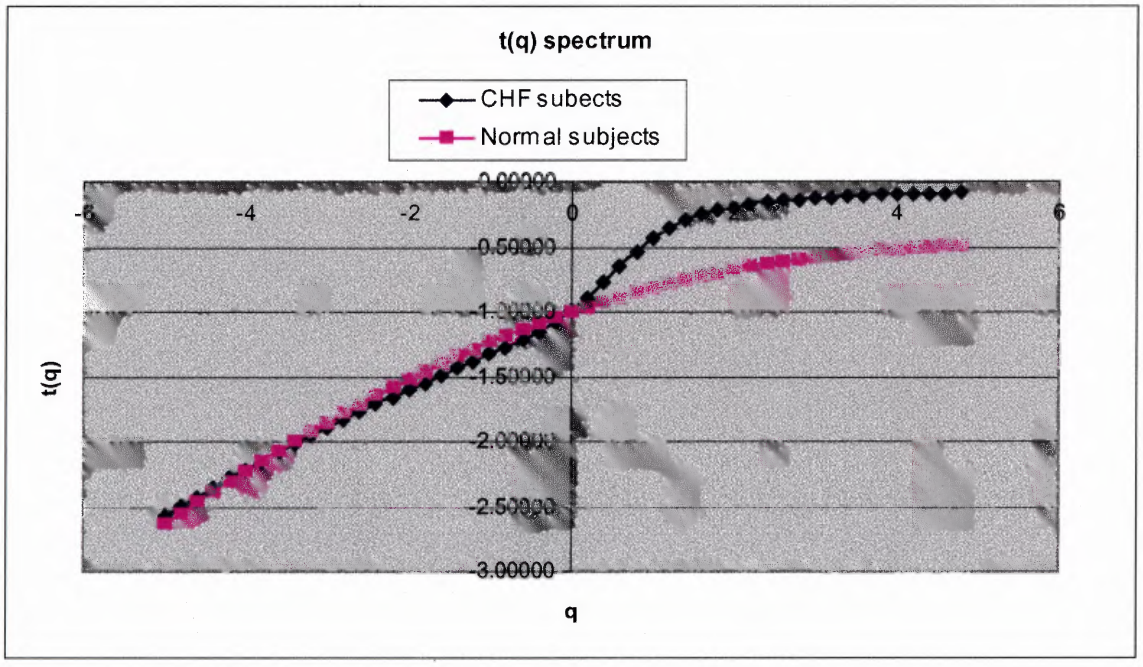

Figure 4.9 Spectrum of τ(q) for 25 CHF and 25 NSR subjects.

Table 4.6 shows mean $\tau(q)$ values for 25 CHF subjects and 25 NSR subjects. Figure 4.9 is $\tau(q)$ spectrum drawn from Table 4.6. The shape of the $\tau(q)$ spectrum is used to differentiate between two groups.

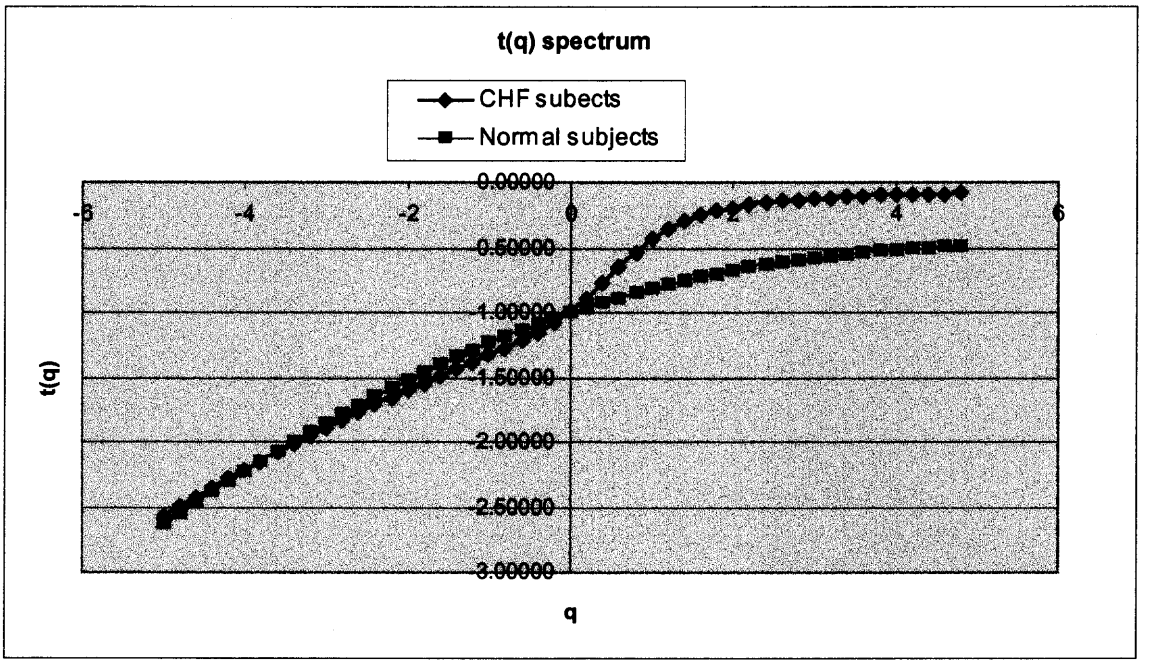

Figure 4.9 Spectrum of $\tau(q)$ for 25 CHF and 25 NSR subjects.

Table 4.6 Mean τ(q) Values for 25 CHF Subjects and 25 NSR Subjects.

q	Mean value of 25 subjects with CHF at indicated resolution of q	Mean value of 25 subjects with NSR at indicated resolution of q
-5	-2.56848	-2.63038
-4.8	-2.49562	-2.54661
-4.6	-2.42382	-2.46405
-4.4	-2.35312	-2.38277
-4.2	-2.28359	-2.30284
-4	-2.21527	-2.22431
-3.8	-2.14820	-2.14724
-3.6	-2.08243	-2.07167
-3.4	-2.01798	-1.99759
-3.2	-1.95488	-1.92503
-3	-1.89309	-1.85397
-2.8	-1.83260	-1.78440
-2.6	-1.77331	-1.71633
-2.4	-1.71515	-1.64977
-2.2	-1.65799	-1.58478
-2	-1.60174	-1.52147
-1.8	-1.54628	-1.45997
-1.6	-1.49157	-1.40045
-1.4	-1.43750	-1.34309
-1.2	-1.38391	-1.28800
-1	-1.33037	-1.23527
-0.8	-1.27585	-1.18488
-0.6	-1.21834	-1.13677
-0.4	-1.15451	-1.09082
-0.2	-1.08018	-1.04687
0	-0.99173	-1.00479
0.2	-0.88780	-0.96444
0.4	-0.77062	-0.92574
0.6	-0.64736	-0.88862
0.8	-0.53093	-0.85306
1	-0.43300	-0.81909
1.2	-0.35601	-0.78675
1.4	-0.29720	-0.75613
1.6	-0.25276	-0.72729
1.8	-0.21908	-0.70031
2	-0.19320	-0.67526
2.2	-0.17291	-0.65215
2.4	-0.15666	-0.63098
2.6	-0.14341	-0.61169
2.8	-0.13244	-0.59420
3	-0.12326	-0.57840
3.2	-0.11551	-0.56417
3.4	-0.10893	-0.55139
3.6	-0.10331	-0.53994
3.8	-0.09849	-0.52969
4	-0.09434	-0.52054
4.2	-0.09077	-0.51240
4.4	-0.08766	-0.50517
4.6	-0.08497	-0.49879
4.8	-0.08263	-0.49317

Table 4.7 shows the t-test performed on the coefficients of the quadratic terms obtained using polynomial fit of second order on CHF and NSR subjects. While Figures 4.10, 4.11 show graphical view of the quadratic fit for both groups.

Table 4.7 T-test of Coefficients of Quadratic Term from the Polynomial Fit Performed on the $\tau(q)$ Spectrum for 25 CHF and 25 NSR Subjects.

t-Test: Two-Sample Assuming Equal Variances		
	Variable 1	*Variable 2*
Mean	-0.015225	-0.02575
Variance	4.9583E-07	1.80567E-05
Observations	25	25
Pooled Variance	9.2762E-06	
Hypothesized Mean Difference	0	
df	6	
t Stat	4.88709611	
P(T<=t) one-tail	0.00137322	
t Critical one-tail	1.94318091	
P(T<=t) two-tail	0.00274645	
t Critical two-tail	2.44691364	

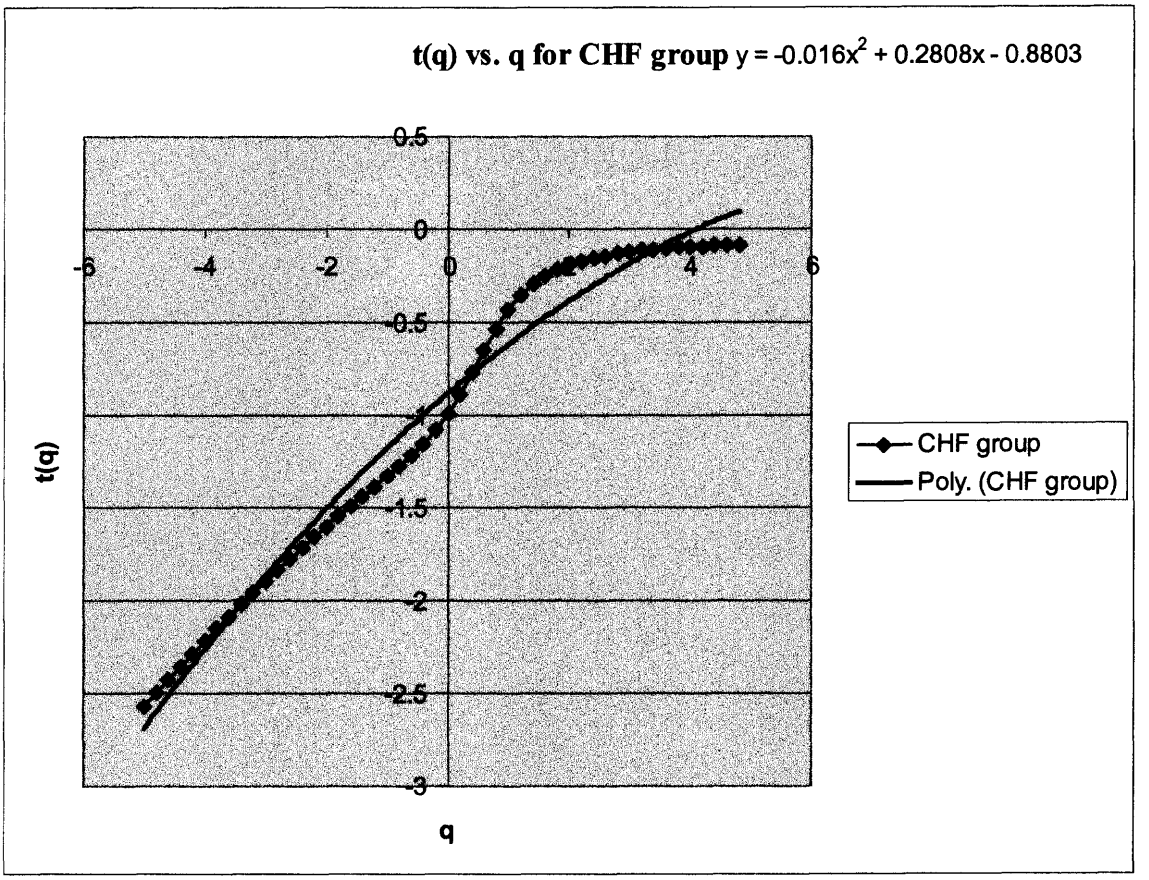

Figure 4.10 Second order polynomial fit in the $\tau(q)$ spectrum of 25 CHF subjects.

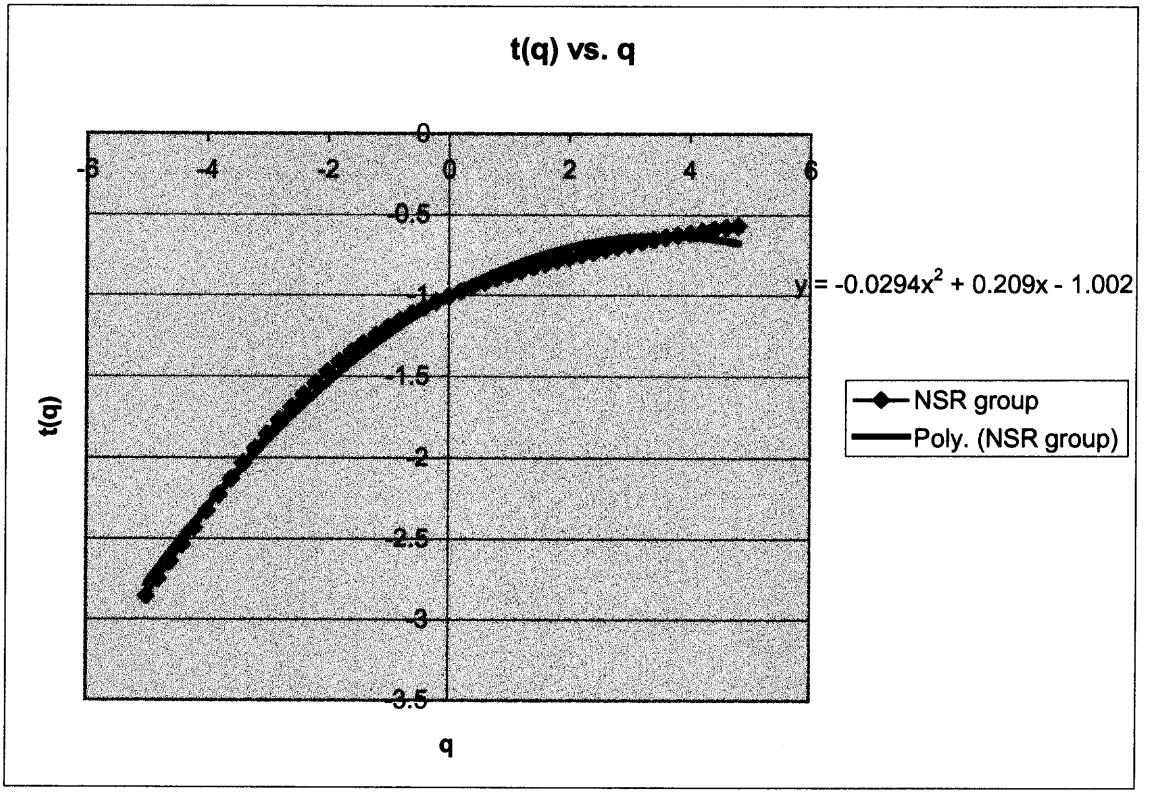

Figure 4.11 Second order polynomial fit in the $\tau(q)$ spectrum of 25 NSR subjects.

Table 4.8 shows mean h values and mean D(h) values for 25 NSR subjects. Table 4.9 shows mean h values and mean D(h) values for 25 CHF subjects (same subjects used to calculate $\tau(q)$). D(h) spectrum is shown in Figure 4.12 to identify NSR subjects (values are taken from Tables 4.8 and 4.9). 25 CHF and 25 NSR subjects have been selected randomly.

Table 4.8 Mean Values of h vs. Mean Values of D(h) for 25 NSR Subjects.

Mean h value for NSR subjects	Mean D(h) values for NSR subjects
0.415817	0.550694
0.409617	0.579813
0.403040	0.609392
0.396141	0.639042
0.388976	0.668408
0.381613	0.697116
0.374128	0.724806
0.366594	0.751173
0.359067	0.776014
0.351574	0.799245
0.344102	0.820913
0.336575	0.841231
0.328855	0.860517
0.320747	0.879141
0.312034	0.897403
0.302543	0.915392
0.292211	0.932915
0.281131	0.949504
0.269546	0.964545
0.257798	0.977469
0.246240	0.987890
0.235163	0.995674
0.224753	1.000915
0.215070	1.003857
0.206068	1.004788
0.197624	1.003969
0.189564	1.001565
0.181693	0.997634
0.173819	0.992117
0.165767	0.984857
0.157409	0.975645
0.148666	0.964259
0.139531	0.950538
0.130068	0.934437
0.120403	0.916066
0.110706	0.895706
0.101165	0.873774
0.091956	0.850774
0.083223	0.827219
0.075058	0.803572
0.067509	0.780203
0.060583	0.757378
0.054257	0.735265
0.048488	0.713945
0.043226	0.693449
0.038423	0.673778
0.034031	0.654913
0.030010	0.636835

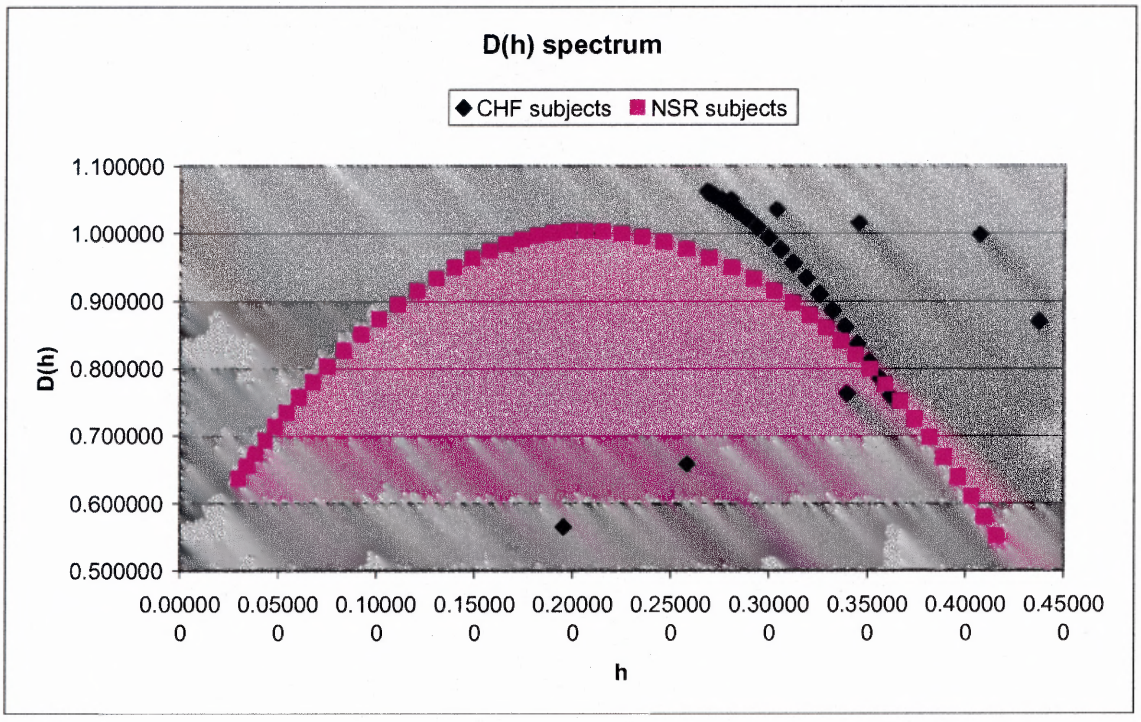

Figure 4.12 D(h) vs. h for 25 CHF and 25 NSR subjects.

Table 4.10 shows the mean $\tau(q)$ values of two healthy subjects from the period of 9 a.m. to 4 p.m. and 12 a.m. to 7 a.m. Figure 4.13 shows the spectrum of $\tau(q)$ for the values taken from Table 4.10 to check the effect of the sleep on multifractality of the heart rate.

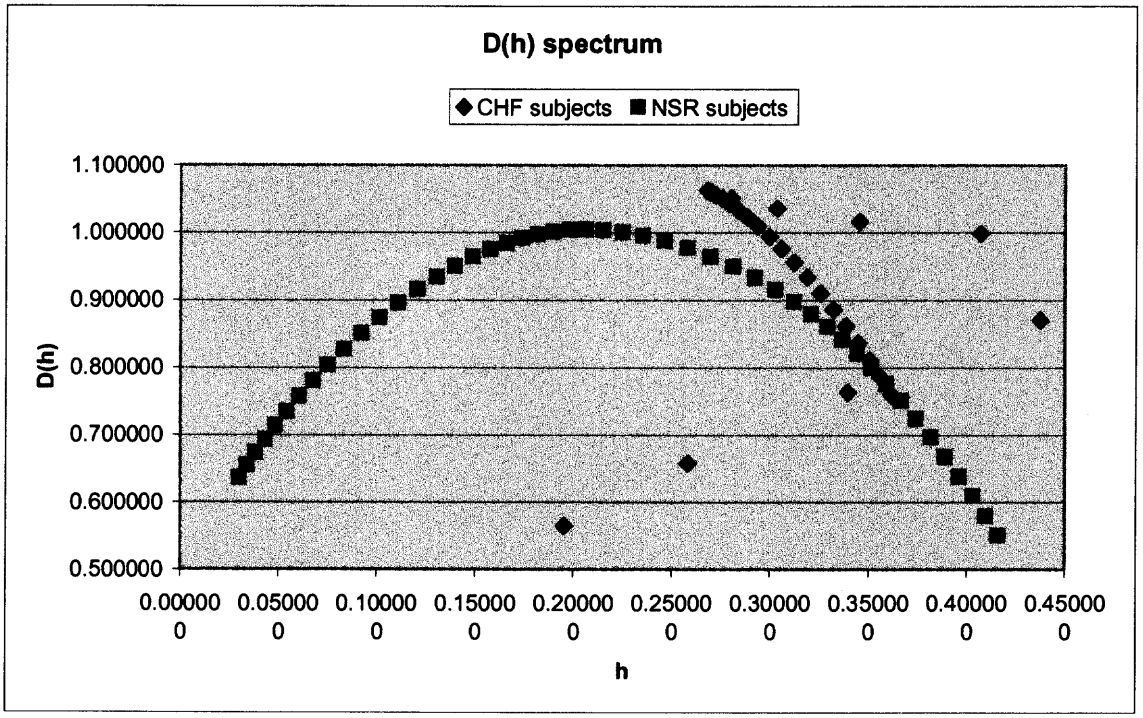

Figure 4.12 D(h) vs. h for 25 CHF and 25 NSR subjects.

Table 4.10 shows the mean $\tau(q)$ values of two healthy subjects from the period of 9 a.m. to 4 p.m. and 12 a.m. to 7 a.m. Figure 4.13 shows the spectrum of $\tau(q)$ for the values taken from Table 4.10 to check the effect of the sleep on multifractality of the heart rate.

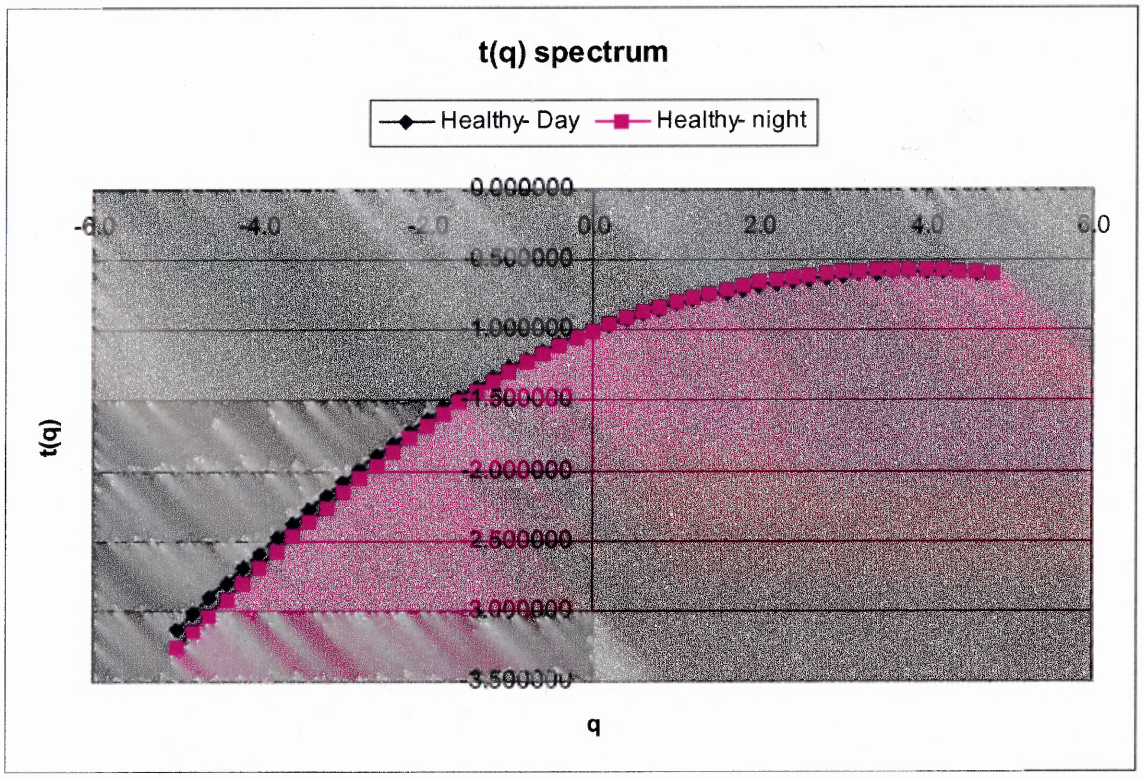

Figure 4.13 Effect of activity on τ(q) for two healthy subjects.

4.5 Discussion

The multifractal analysis was performed on the normal subjects and subjects with CHF. From the graphs in Figures 4.1 and 4.2, we can infer that there is no significant change in the shape of the singularity spectrum due to the change in the order of the Gaussian derivative. Performed analysis indicates that a wide range is obtained for D(h) in the NSR group and a narrower range is obtained for D(h) for the CHF group. Since there is no significant effect of the Gaussian derivative, analysis was performed using Gaussian derivative 3.

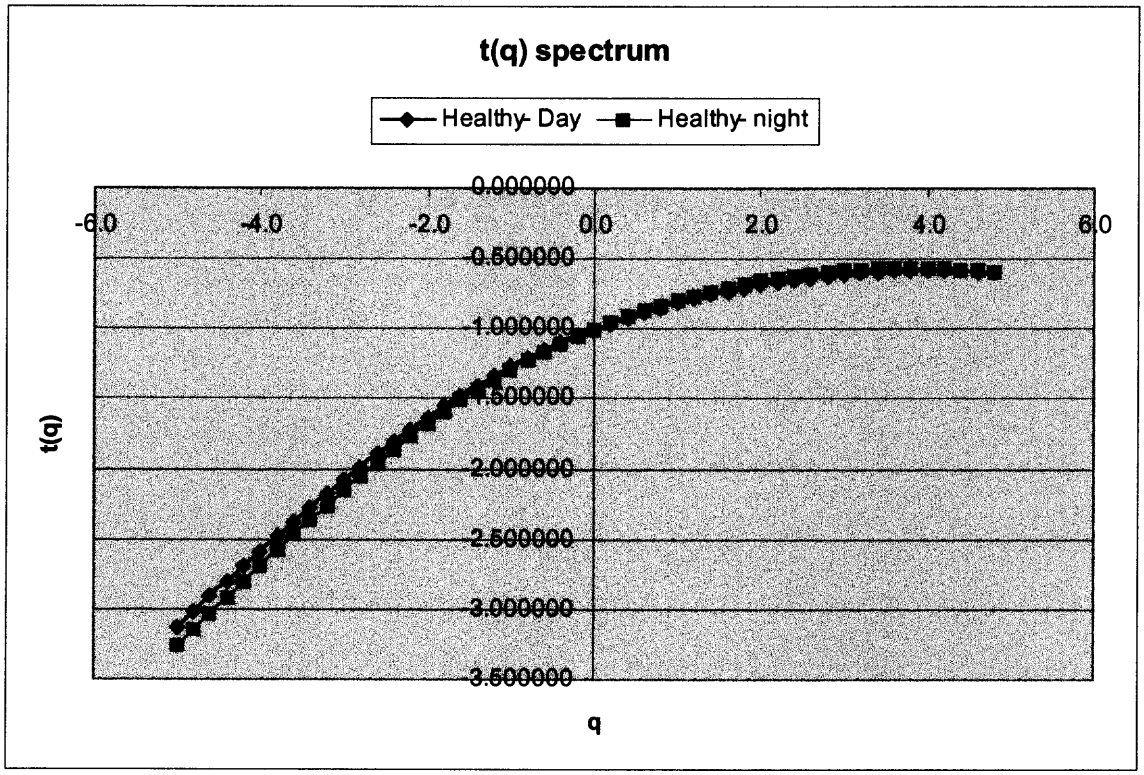

Figure 4.13 Effect of activity on $\tau(q)$ for two healthy subjects.

4.5 Discussion

The multifractal analysis was performed on the normal subjects and subjects with CHF. From the graphs in Figures 4.1 and 4.2, we can infer that there is no significant change in the shape of the singularity spectrum due to the change in the order of the Gaussian derivative. Performed analysis indicates that a wide range is obtained for D(h) in the NSR group and a narrower range is obtained for D(h) for the CHF group. Since there is no significant effect of the Gaussian derivative, analysis was performed using Gaussian derivative 3.

From the data of Tables 4.3, 4.4 and 4.5, it is determined that a minimum of 30,000 points are required in order to perform analysis without error. Figures 4.3, 4.4, 4.5 and 4.6 illustrate that a minimum of 30000 points are required to distinguish between the two data sets (CHF and NSR). For NSR group, $\tau(q)$ spectrum demonstrates nonlinear behavior for 30000 and more data points and shape of the $\tau(q)$ spectrum is also preserved. For CHF subjects, there is no change in the $\tau(q)$ spectrum for 30000 and more data points.

There is a significant change in the graph of $\tau(q)$ vs. q and D(h) vs. h between NSR group and CHF group (Figures 4.9 and 4.12). As discussed in the theory, the RR interval time series for a healthy subject demonstrate multifractal behavior. Whereas, the RR time series for a subject with CHF demonstrate monofractal behavior. The $\tau(q)$ spectrum exhibits a non-linear behavior for the NSR group, whereas, the $\tau(q)$ spectrum exhibits comparatively linear behavior for the CHF group. Polynomial fit of the second order was used to check the non-linearity of the $\tau(q)$ spectrum for both CHF and NSR groups. The value of the coefficient of the quadratic term is close to zero for CHF subjects than NSR subjects. That is, $\tau(q)$ is linear comparatively for the CHF group than NSR. T-test was performed on the coefficients of the quadratic term for 25 CHF and 25 NSR subjects. From Table 4.7, $P = 0.00137$ (one tail) < 0.05 and $P = 0.00274$ (two tail) < 0.05. This shows that there is significant difference between the coefficient values of the quadratic term between two groups. Figures 4.10 and 4.11 shows graph of the quadratic fit in the $\tau(q)$ spectrum of both groups. Of the $\tau(q)$ spectrum of the obtained data for the particular group is nonlinear means a subject is normal, while if the $\tau(q)$ spectrum of the obtained data is linear means a CHF subject. However, it is hard to

distinguish CHF subjects and NSR subjects just by analyzing $\tau(q)$ spectrum. The D(h) spectrum provides alternate way to identify subjects of both groups. The D(h) spectrum has broad range of singularities-*h* for NSR group, while range gets narrower for the CHF subjects. Thus, the D(h) spectrum easily distinguishes both NSR group and CHF group.

The multifractality of the heart beat dynamics cannot be explained by activity [26]. That is, the shape of the $\tau(q)$ spectrum will remain unchanged even if we perform multifractal analysis, on RR interval time series, on the same subject by collecting data during activity and data without doing any activity. For this study, the nighttime sleep data and data without doing any activity in the daytime were taken. As discussed before, the mean values of $\tau(q)$ (from two healthy subjects) were obtained on both types of data (daytime and sleep) to validate the effect of sleep on multifractality of the heart rate signal. The results of the analysis proved that there is no significant change in the $\tau(q)$ spectrum due to the sleep. Mean values of $\tau(q)$ vs. q are depicted in the Table 4.9. As seen in Figure 4.13, the $\tau(q)$ spectrum curve generated for the daytime data and nighttime data overlap each other.

CHAPTER 5

CONCLUSION AND FUTURE WORK

5.1 Conclusion

Most pervious characterizations of the HRV have relied upon the conventional methods such as time domain, frequency domain and power spectrum analysis. In this work, it is shown that the WTMM method of multifractal analysis based on nonlinear dynamics is accurate and reliable. Wavelet transform modulus-maxima tracking gives direct access to the D(h) singularity spectrum of any fractal signal and easily distinguish multifractal signals and monofractal signals. Since the fractal behavior decreases in the subjects with the heart diseases, the heart rate signal looses its multifractality and it is easily detected by the WTMM method of multifractal analysis.

Eventually, the goal of this thesis was to differentiate normal subjects from congestive heart failure subjects by applying nonlinear dynamics method multifractal analysis and it was successfully achieved by testing the linearity and nonlinearity of the $\tau(q)$ spectrum and by the shape of the D(h) spectrum. The nonlinearity test was performed using polynomial fit of second order on the data of $\tau(q)$. The values of the coefficients of quadratic terms for the CHF subjects are comparatively lower than NSR subjects. That is, stronger linearity in the $\tau(q)$ spectrum of CHF group and heart rate signal is less multifractal. From the t-test result ($P = 0.00137$ for one tail and $P = 0.00274$ for two tail), it is concluded that there are major changes in the coefficients of the quadratic term between CHF subjects and NSR subjects. In study 1, results showed that there is no effect of the Gaussian derivative on the shape of the singularity spectrum. Results

showed that there was a shift in the curve of D(h) for both NSR and CHF groups but no major change in shape was found. The second study was conducted to discover the requirements of the minimum data points and to check the effect of the length. A total 30 subjects were selected for this test and 28 successful (0.93% success ratio) results were obtained out of 30 by comparing the $\tau(q)$ and the D(h) spectrum with the increment of 10000 data points starting from 10000 to 90000. From the results we can conclude that minimum of 30000 data points are required to obtain appropriate results in multifractal analysis. Moreover, for 30000 and onwards data points, curve of the $\tau(q)$ spectrum preserved its shape. To differentiate the NSR subjects from CHF subjects, study was conducted on 25 NSR subjects and 25 CHF subjects. A total of 47 subjects, out of 50, were identified and placed in the appropriate group by applying multifractal analysis method on each subject and evaluating the shape of the D(h) spectrum and nonlinearity of the $\tau(q)$ spectrum. Thus, the success ratio to differentiate between NSR group and CHF group is 0.94%, while 0.06% unsuccessful results were obtained. In conclusion we can say that multifractal analysis is appropriate method to distinguish healthy subjects from CHF subjects. Results showed that there is a major change in the D(h) spectrum for the NSR subjects and the CHF subjects. From the results of the sleep data and daytime data in the last task, we can conclude that there is no effect of sleep on the multifractal behavior of the heart rate signal. Eventually, the goal of the analysis was carried out successfully.

The major draw back of this method is that minimum of data required is approximately for six hours. It cannot predict pathological or normal condition by analyzing short time data.

5.2 Future Work

It is not surprising that the nonlinear method, multifractal analysis, is far from being applied in everyday clinical practice. Data from clinical studies should be exchanged such that data can be merged and analyzed in different laboratories with competing methods. The format of the data for this method should be appropriate in a way that those should work in all different computer environments such as Windows, Unix, and Linux. Furthermore, code should be available in all different languages (MATLAB, C++, JAVA and so on) so that any of the computer programs should execute them. Furthermore, more accurate algorithms are still required for this method. Very few resources are available for the WTMM method of multifractal analysis, which is a major drawback of the research because students/researchers are afraid to involve in this research due to the lack of the resources.

The use of this method in clinical world is highly depended upon the effectiveness of multifractal analysis to distinguish other pathologies such as myocardial infraction, atrial fibrillation, ventricular dysfunction, and significant arrhythmias. Deep Multifractal analysis study is still required in mentioned pathologies.

APPENDIX A

PROGRAMS USED IN MULTIFRACTAL ANALYSIS

This appendix contains programs used in this study, which are written in MATLAB 7.0 and in C language. Program A is written in MATLAB. Programs B and C are written in C language. Program A was used to deglitch the RR interval time series. Program B was used to calculate the multifractal partition functions of a time series. Program C was used to calculate the tau(q) spectrum and the multifractal spectrum, D(h). Input to each of the main program is a text file with RR intervals arranged in two columns. First column is the index and second column contain the values of the RR intervals.

Program A To deglitch the RR interval time series

```
function datum=deglitching(vals)
 [a,b]=size(vals);
times(1)=vals(1);
for i=2:a
  times(i)=times(i-1)+vals(i);
end
labels=ones(a,b);
 [labs,resids] = ardeglch(vals, labels);
c=1;
for i=1:a
   if labs(i)==1
      datum(c,1)=vals(i);
     c=c+1;

end
end
function [labs,resids] = ardeglch(data, inlabels, modelorder, iqrcrit)
% labs = arresid(data, inlabels, modelorder, iqrcrit)
% identifies outliers in a time series by
% looking at the residuals of a forward and
% backward AR fit.
% Excludes from the fit beats labeled 0 in <inlabels>
% iqrcrit gives the criteria in inter-quartile range units
      % for an outlier.
% Returns a vector of the same length as the data which
% contains a 0 for any beat marked as bad either in inlabels
% or from the AR fit.
% [labs,resids] = ardeglch...
% gives the actual values of the residuals as an optional second argument
if nargin < 3
  modelorder = 3;
```

```
end
if nargin < 4
  iqrcrit = 3.5;
end
% fit the forward model
labforward = arresid(data, inlabels, modelorder);
% fit the backward model
labbackward = arresid( data((length(data)):-1:1), inlabels((length(data)):-1:1), modelorder);
% take the smaller of the two residuals, remembering
% to put labbackward back in forward order.
labels = min(labforward, labbackward(length(data):-1:1) );
resids = labels;
% Compute the interquartile range and limits for outliers.
lims = prctile(labels,[25 50 75]);
iqrange = lims(3) - lims(1);
bottom = lims(1) - iqrange*iqrcrit;
top = lims(3) + iqrange*iqrcrit;
% bogus points are marked as 666666 in <labels> or as 0 in <inlabels>
labs = (labels > bottom & labels < top & labels ~= 666666 & inlabels ~= 0 );

function resids = arresid(data, inlabels, modelorder)
% res = arresid(data, inlabels, modelorder, outcrit)
% Identifies outliers in a time series by looking
% for outliers to a linear prediction model
% data -- the time series
% inlabels -- a zero for each already-known bogus data item
% modelorder -- what model order to use
% returns resids --- the residuals written in terms of IQRs from the median
% These are synchronized to the data point being predicted.
% Convert to a column format
data = data(:);
inlabels = inlabels(:);
if length(inlabels) ~= length(data)
  error('arresid: data and labels must be the same length.');
end
% create a lag-embedded matrix of preimages
pre = ones( length(data) - modelorder, modelorder+1);
lpre = ones( length(data) - modelorder, modelorder+1);
% and the images of this
targs = data( (modelorder+1):(length(data)) );
% fill in the matrix
for k=1:modelorder
  foo = length(data) - modelorder;
  pre(:,(k+1)) = data( (modelorder+1-k):(length(data)-k) );
  lpre(:,(k+1)) = inlabels( (modelorder+1-k):(length(data)-k) );
end
lpre(:,1) = inlabels( (modelorder+1):(length(data)) );
% note that the matrix <pre> has all ones in the first column,
% to handle the constant part of the linear model
% the <lpre> matrix gives the labels of the correspond entries
% in <pre>
% get rid of the known bad beats
% by identifying any row with a bad beat
goodrows = find( all((lpre~= 0)' )');
% The following is for version 5
%goodrows = find( all((lpre~= 0),2) );
```

```
% create matrices for the preimages and targets that have
% only clean beats
cleanpre = pre(goodrows,:);
cleantargs = targs(goodrows);
% fit the linear model
params = cleanpre\cleantargs;
% calculate the residuals
res = targs - pre*params;
% set the output to give the residual for the beat being
% predicted.  Make bogus residuals big so they
% are easily pulled out
% Magic number 666666 is used in other programs
resids = 666666*ones(size(data));
resids( (modelorder + 1):(length(data)) ) = res;
```

Program B To calculate the multifractal partition functions of the RR interval time series.

```
#include <stdio.h>
#include <math.h>
#include <values.h>
#include <stdlib.h>
#include <string.h>

#define SQR(x) ( (x) * (x) )
#define Min(x,y) ( ((x) < (y)) ? (x) : (y) )
#define Max(x,y) ( ((x) > (y)) ? (x) : (y) )
#define SIGN(x) (((x)>0.0)?(1):(-1))
#define SIGN1(x) (((x)<0.0)?(-1):(1))

#define EPS 1e-4
#define EPS1 1e-6
#define MAX_CHAR_IN_LINE 4096
#define STRL    80
#define PI M_PI
#define Pi2 2.0*PI
#define NumOfArgc 5     /* Number of arguments called by the executable file */
#define TimesWS 6       /* The factor of convolution range; i.e., wavelet
                                box =-TimesWS*WS..TimesWS*WS */
#define Ratio (1.0/8.0) /* Defines the ratio between maximum scale (wavelet
                                box) and signal length */
#define DQ 0.2              /* Resolution of moments q */


/* SUBROUTINE PrintColor

  Prints the color cascade in a ppm format (can be read by xv or ImageMagick).

  Subroutine for constructing color coded 3D wavelet decomposition:
  x axis is time; y axis is wavelet  scale; z axis is wavelet coefficient
  (bright colors represent large values).
*/

PrintColor(double *vec, long i, long nx, long ny, double max, double min)
{
   long l, j, bin, color1, color2, color3, N, N1, N2, N3, N4, N5, N6;
```

```
    double delta;

    N = 255;
    N1 = N;
    N2 = 2*N;
    N3 = 3*N;
    N4 = 4*N;
    N5 = 5*N;
    N6 = 6*N;

    delta = (max - min)/(double)(N6-2);

    printf("P3\n# CREATOR: multifractal\n%d %d\n255\n", nx, ny);

    j = l = 0;
    while (l < i) {
      bin  =  (long)(((vec[l] - min)/delta));

      if (bin < N1) {
              color1 = N;
        color2 = bin;
              color3 = 0;
            }
            else if (bin < N2) {
              color1 = N2-bin;
              color2 = N;
              color3 = 0;
            }
            else if (bin < N3) {
              color1 = 0;
              color2 = N;
              color3 = bin-N2;
            }
            else if (bin < N4) {
              color1 = 0;
              color2 = N4-bin;
              color3 = N;
            }
            else if (bin < N5) {
              color1 = bin-N4;
              color2 = 0;
              color3 = N;
            }
            else {
              color1 = N;
              color2 = 0;
              color3 = N6-bin;
            }
            printf("%3d %3d %3d ", color1, color2, color3);
            l++;
            if (++j >= 5) {
              printf("\n");
              j = 0;
            }
    }
}
```

```
/* SUBROUTINE F

   Calculates continuous Gaussian wavelet functions (zero to 7th derivative).
*/

double F(long n, double t)
{
  switch (n) {
    default:
    case 0:  return exp(-0.5*SQR(t));
    case 1:  return -t*exp(-0.5*SQR(t));
    case 2:  return (-1+t*t)*exp(-0.5*SQR(t));
    case 3:  return t*exp(-0.5*SQR(t))*(3-t*t);
    case 4:  return exp(-0.5*SQR(t))*(pow(t,4.0)-6*t*t+3);
    case 5:  return -t*exp(-0.5*SQR(t))*(pow(t,4.0)-10*t*t+15);
    case 6:  return exp(-0.5*SQR(t))*(pow(t,6.0)-15*pow(t,4.0)+45*t*t+15);
    case 7:  return -t*exp(-0.5*SQR(t))*(pow(t,6.0)-21*pow(t,4.0)+105*t*t-105);
  }
}


/* SUBROUTINE  PrepareVecF

   Vector storing the values of the wavelet function; done for numerical
   efficiency
*/

void PrepareVecF( double ws, double vec[], long Derivative )
{
  long i, tempi = (long)((double)TimesWS*ws);

  for (i = 0; i <= 2*tempi; i++)
     vec[i] = F((long)Derivative,((double)i-(double)(tempi))/ws);
}

/* SUBROUTINE MF1


   Find the maximum for the scale window ws, by performing the following steps:
    1) Wavelet convolution of the signal for increasing wavelet scale.
    2) Locate the local maxima of the absolute value of wavelet
       coefficient as a function of time for each wavelet scale.
    3) Check whether a local maximum at a given wavelet scale is located
       close to a maximum at a smaller scale - if yes connect both maxima,
       otherwise cancel it. Generate maxima lines.
    4) Check that the number of maxima at larger scales is less or equal
       to that at a smaller scale.
    5) Track maxima lines for increasing wavelet scale by choosing at each
       scale value the supremum between all previous values at smaller
       scales.
*/

double MF1(double *vec, long n, double min_q, double max_q, double dq,
           double min_ws, double max_ws, double dws, long Derivative, long code)
```

```
{
  long nq,i,i1,i2,j,jj,sign,sign1,tempi_max,tempi,tempi1,tempi2,n_max,icolor;
  double *s, s1, min, max, temp, temp1, temp2, q;
  double *MaxVec, *VecWL, *VecF, *VecColor, *pt, ws;
  long *VecWLX, *MaxVecX, *ptl;

  nq = (long)((max_q-min_q)/dq)+1;

  MaxVec = (double *)calloc((size_t)(n+1),(size_t)(sizeof(double)));
  MaxVecX = (long *)calloc((size_t)(n+1),(size_t)(sizeof(long)));
  tempi_max = (long)((double)TimesWS*max_ws);
  s = (double *) calloc( (size_t)(nq+1),sizeof(double) );
  VecF = (double *) calloc( (size_t)(2*tempi_max+1),sizeof(double) );
  VecWL = (double *) calloc( (size_t)(n+1),sizeof(double) );
  VecWLX = (long *) calloc( (size_t)(n+1),sizeof(long) );

  if (code == 1) {
        printf("# %f\n", min_q);
        fflush(NULL);
  }
  else if (code == 3) {
        for (ws = min_ws, tempi1 = 0; ws <= max_ws; ws *= dws)
          tempi1++;
        icolor = 1;
        max = -1e20;
        min = 1e20;
        VecColor = (double *)calloc((size_t)((n-2*tempi_max-1)*tempi1+1),
                                        sizeof(double));
  }
  jj=0;
  for (ws = min_ws; ws <= max_ws; ws *= dws) {
        tempi = (long)((double)TimesWS*ws);
        for (i = 0; i < (2*tempi+1); i++)
          VecF[i] = 0.0;
        for (i = 0; i < (n+1); i++)
          VecWL[i] = 0.0;
        for (i = 0; i < (n+1); i++)
          VecWLX[i] = 0;
        PrepareVecF(ws, VecF, Derivative);

        /* do the convolution */
        for (i = tempi_max; i < (n-tempi_max-1); i++) {
          s1 = 0.0;
          for (j = i-tempi; j <= (i+tempi); j++)
                s1 += vec[j] * VecF[j-i+tempi];
          VecWL[i] = fabs(s1/ws);
          if (code == 3) {
                VecColor[icolor] = VecWL[i];
                icolor++;
                if (max < VecWL[i])
                  max = VecWL[i];
                if (min >VecWL[i])
                  min = VecWL[i];
          }
        }
```

```
        /* Find the local maxima of the wavelet coefficient for each scale  */
        n_max = 0;
        sign = SIGN(VecWL[tempi_max+1] - VecWL[tempi_max]);
        temp1=0.0;
        for (j = 0, i = tempi_max+2; i < (n-tempi_max-1); i++) {
           if ((fabs(VecWL[i] - VecWL[i-1]) > 0.0) &&
                    ((sign == 1) && ((SIGN(VecWL[i] - VecWL[i-1])) == (-1)))) {
                    temp = VecWL[i-1];
                    if (code == 2) {        /* Print the maxima lines (code 2) */
                       printf("%d %g\n", i, log(ws)/log(10.0));
                       fflush(NULL);
                    }
                    n_max++;
                    VecWL[j]=temp;
                    VecWLX[j]=i-1;
                    temp1=temp;
                    j++;
           }
           sign=SIGN(VecWL[i]-VecWL[i-1]);
        }

        /* Tracking the maxima lines: test for supremum */
        if (ws > min_ws) {
           for (i1 = i2 = i = 0; i < nq;i++)
                    s[i]=0.0;
           while (((i1-1) < n_max) && ((i2-1) < jj)) {
                    if ((VecWLX[i1] - MaxVecX[i2]) <= (MaxVecX[i2+1] - VecWLX[i1]))
                       VecWL[i1] = Max(VecWL[i1],MaxVec[i2]);
                    else
                       VecWL[i1] = Max(VecWL[i1],MaxVec[i2+1]);
                    for (i = 0; i < nq; i++)
                       s[i] += pow(VecWL[i1], min_q+(double)i*dq);
                    i1++;
                    i2++;
                    while ((i2 < jj) && (VecWLX[i1] >= MaxVecX[i2]))
                       i2++;
                    i2--;
           }
           if (code == 1) {        /* Print the partition function */
                    printf("%g ", log(ws)/log(10.0));
                    for (i = 0; i < nq; i++)
                       printf("%g ", log(s[i])/log(10.0));
                    printf("\n");
                    fflush(NULL);
           }
        }
        jj = n_max;
        pt = MaxVec;
        MaxVec = VecWL;
        VecWL = pt;
        ptl = MaxVecX;
        MaxVecX = VecWLX;
        VecWLX = ptl;
}
free(VecF);
free(VecWL);
```

```
    free(VecWLX);
    free(MaxVec);
    free(MaxVecX);

    /* Print the wavelet cascade (code 3) */
    if (code == 3) {
            PrintColor(VecColor,icolor,n-2*tempi_max-1,tempi1,max,min);
            free(VecColor);
    }
}


main(int argc, char *argv[])
{
    long i, j;
    long N, Derivative = 3, code = 1;
    double *VecX, temp, tempx, tempy, ws, dw, MinScale, MaxScale,
            q, q_min, q_max, dq;
    FILE *fp;

    if (argc < NumOfArgc) {
      printf("Usage: %s INPUT N QMIN QMAX DW MODE >OUTPUT\n", argv[0]);
      printf("  INPUT  name of file containing the input time series\n");
      printf("  N      number of points (lines) in INPUT\n");
      printf("  QMIN   minimum MF order\n");
      printf("  QMAX   maximum MF order\n");
      printf("  DW     order of the Gaussian derivative wavelet (0-7)\n");
      printf("  MODE   the type of output to be produced, one of:\n");
      printf("           1: partition functions (text)\n");
      printf("           2: maxima lines (text)\n");
      printf("           3: wavelet cascade (PPM image)\n\n");
      printf(" INPUT is a text file containing two columns of numbers; the\n");
      printf(" first is ignored, and the second contains the data values.\n");
      exit(0);
    }

    /* N is the series length */
    N = atol(argv[2]);

    /* VecX is the vector  storing the data */
    VecX = (double *) malloc((size_t)(N+1) * sizeof(double));

    for (i = 0; i < N+1; i++)
            VecX[i] = 0.0;

    /* Open data file for reading two column data file. The second column
       should be the data that are analyzed. */
    fp = fopen( argv[1], "r");
    for (i = 0; (i < N) && (fscanf(fp, "%lf%lf", &temp, &(VecX[i])) == 2); i++)
            ;
    fclose(fp);
    N = i;

    /* MaxScale is the maximum scale analyzed */
    MaxScale = Ratio*0.5*(((double)N)-1.0)/(double)TimesWS;
    /* MinScale is the minimum scale analyzed */
```

```
    MinScale = 2.0;    /* 0.5*M_E */
    /* q_min is the minimum moment q for which the partition function is
       calculated */
    q_min = atof(argv[3]);
    /* q_max is the maximum moment q for which the partition function is
       calculated */
    q_max = atof(argv[4]);
    /* resolution of moments in steps dq for which the partition function is
       calculated */
    dq = DQ;
    if (argc > NumOfArgc) {
            Derivative = atoi(argv[5]);
            if (argc > (NumOfArgc+1))
               code = atoi(argv[6]);
    }
    /* scale resolution for which the partition function is calculated */
    dw = pow(2.0,0.05);
    MF1(VecX, N, q_min, q_max, dq, MinScale, MaxScale, dw, Derivative, code);
    free(VecX);
```

Program c: To calculate the tau(q) and singularity spectrum

```
BEGIN{
  s0=0.0;
  s1=s2=0.0;
  dq=0.2;
}
{
  if (NR==1)
    {
# read the data
     q_min=$2;
     for (i=1;i<NF;i++)
       {
            t0[i]=0.0;
            t1[i]=0.0;;
          }
    }
  else
    {
# Fits the partition function is the desire range
     if (($1>=a)&&($1<=b))
       {
         x=$1;
            s0++;
            s1+=x;
            s2+=x*x;
            for (i=2;i<=NF;i++)
              {
                t0[i-1]+=($i);
                t1[i-1]+=x*($i);
              }
       }
    }
}
END{
  for (i=1;i<NF;i++)
```

```
   {
# print tau(q) spectrum.
     q[i]=q_min+(i-1)*dq;
     tau[i]=(t1[i]*s0-s1*t0[i])/(s0*s2-s1*s1);
     print q[i],tau[i];
   }
  print "& &";
# print the D(h) spectrum
  for (i=2;i<(NF-1);i++)
    print (tau[i+1]-tau[i-1])/(q[i+1]-q[i-1]),
              (tau[i+1]-tau[i-1])/(q[i+1]-q[i-1])*q[i]-tau[i];
}
```

REFRENCES

1. http://info.med.yale.edu/images/ heart_anatomy.html. Retrieved on 25 May 2005.

2. http://www.cardioconsult.com/Physiology/. Retrieved on 25 June 2005.

3. http://webcenter.health.webmd.netscape.com/content/pages/9.html. Retrieved on 25 June 2005.

4. Elaine N. Marieb, "Human Anatomy and physiology," Benjamin and Cummings, 1989.

5. http://www.physionet.org/tutorials/ndc/. Retrieved on 25 May 2005.

6. http://www.healthyhearts.com/ecg/normalecg.htm. Retrieved on 5 July 2005.

7. L. Sherwood, "Human Physiology From Cells to Systems," Books/Cole, 2001.

8. http://www.cbi.dongnocchi.it/glossary/RR.html. Retrieved on 28 June 2005.

9. E. Toledo, "Linear and Nonlinear Characteristics of the Human ECG as Markers for Cardiovascular Functioning," Tel Aviv University Raymond and Beverly Sackler Faculty of Exact Sciences School of Physics and Astronomy Abramson Center for Medical Physics, 2002;2-35.

10. S. Akselrod, "Components of Heart Rate Variability: Basic Studies," Futura Publishing, 1995.

11. J. Smith, and J. Cohen, "Simple finite-element model accounts for wide range of cardiac dysrhythmias," Proc Natl Acad Sci, 1984;81:233-7.

12. A. L. Goldberger, V. Bhargava, B. J. West, and A. J. Mandell, "Some observations on the question: Is ventricular fibrillation chaos?," Physica D, 1986;19:282-9.

13. D. Rigney, and A. L. Goldberger, "Nonlinear mechanics of the heart's swinging during pericardial effusion," American Journal of Physiology, 1989;257:H:1292-1305.

14. S. M. Ryan, A. L. Goldberger, S. M. Pincus, J. Mietus, and L. A. Lipsitz, "Gender- and age-related differences in heart rate dynamics: are women more complex than men?," Journal of American College of Cardiology, 1994; 24:1700-1707.

15. http://reylab.bidmc.harvard.edu/tutorial/DFA/node3.html. Retrieved on 25 May 2005.

16. L. A. Lipsitz, and A. L. Goldberger, "Loss of "complexity" and aging: potential applications of fractals and chaos theory to senescence," Journal of American Medical Association, 1992;267:1806-9.

17. http://ccforum.com/content/8/6/R367. Retrieved on 28 June 2005.

18. R. Furlan, S. Guzzetti, W. Crivellaro, S. Dassi, M. Tinelli, G. Baselli, S. Cerutti, F. Lombardi, M. Pagani, and A. Malliani, "Continuous 24-hour assessment of the neural regulation of systemic arterial pressure and RR variabilities in ambulant subjects," Circulation, 1990; 81:537-547.

19. P. Ivanov, A. Luis, A. L. Goldberger, H. Shalomo, H. E. Stanley, and Z. Struzik, "From 1/f noise to multifractal cascades in heartbeat dynamics," Chaos, 2001;11: 641-645.

20. A. J. Seely, and P. Macklem, "Complex systems and the technology of variability analysis," Critical Care, 2004; 8:R367-R384.

21. H. E. Stanley, L. A. Amaral, A. L. Goldberger, S. Havlin, P. Ivanov, and C. K. Peng, "Statistical physics and physiology: monofractal and multifractal approaches," *Physica A,* 1999; 270:309-324.

22. Y. G. Sinai, J. Russ. Math. Surveys 166 (1972) 21.

23. http://www.physionet.org/tutorial/multifractal. Retrieved on 20 January 2005.

24. http://www.math.vt.edu/people/hoggard/FracGeomReport/node3.html. Retrieved on 20 January 2005.

25. http://www.physionet.org/physiotoolkit/multifractal. Retrieved on 16 December 2004.

26. E. Bacry, J. F. Muzy and A. Arneodo, "Multifractal formalism for fractal signals: The structure-function approach versus the wavelet-transform modulus-maxima method," Physical Review E, 1993; 47:875-884.

27. P. Goupillaud, A. Grossmann and J. Morlet, "Cycle-octave and related transforms in seismic signal analysis," Geoexploration, 1984; 23:85-102.

28. M. Holschneider, Thesis, University of Aix-Marseille II, Journal of Statistical Phys., 1988; 50-963.

30. http://www.mathjmendl.org/chaos/. Retrieved on 25 May 2005.

31.http://www.bearcave.com/misl/misl_tech/wavelets/hurst/random_walk.html. Retrieved on 5 July 2005.

32. C. Tu, and W. Hwang, "Analysis of Singularities From Modulus Maxima of Complex Wavelets," IEEE Transaction on Information Theory, 2005; 51:1049-1062.

33. http://www.physionet.org/tutorials/multifractal. Retrieved on 16 December 2004.

34. http://www.math.vt.edu/people/hoggard/FracGeomReport/node3.html. Retrieved on 25 May 2005.

35. M. Holschneider, J. Stat. Phys. 50, 963 (1988); Thesis, University of Aix-Marseille II, 1988.

36. S. M. Ryan, A. L. Goldberger, S. M. Pincus, J. Mietus, and L. A. Lipsitz, "Gender- and age-related differences in heart rate dynamics: are women more complex than men?," Journal of American College of Cardiology, 1994; 24:1700-1707.

37. http://www.healthyheart.org/images. Retrieved on 6 July 2005.